On-Orbit Manufacturing Using Solid Foams

Authored by Peter G.B. Hastie

James Watt School of Engineering

University of Glasgow

Signature of Author: _____

Date: _____

Abstract

There is growing interest in the development of processes that can enable the manufacturing of products in space. In-space manufacturing could remove the limitations imposed by terrestrial manufacturing and the launch environment on products used in space and enable large-scale space infrastructure that could further develop in-space capabilities. Examples of large-scale space infrastructure, that could be enabled by in-space manufacturing, include large solar arrays, or orbital reflectors, to increase the amount of light on terrestrial solar arrays. Given the large scale of the proposed infrastructure made using in-space manufacturing and the large energy demands that such construction would place on a space mission, materials that have a low energy consumption for each unit of volume or mass constructed could present advantages for an in-space manufacturing facility. This thesis examines the use of solid foams, which typically require much less energy to apply, to construct an equivalent volume of engineered plastics or metals.

To explore the development of in-space manufacturing and solid foam manufacturing, this thesis presents a literature review based on these fields. A trade-off review is also conducted to compare the material properties and process characteristics of a range of potential in-space manufacturing processes and the materials that they are capable of producing, to understand what characteristics are important for an in-space manufacturing facility. Case studies were used to understand if solid foams could provide an advantage for products manufactured in-space. Two generalised use cases were explored, one structural and one thermal, where each was an abstract use case that was not bound by a specific mission, as well as a specific use case, in which the solid foam was intended for a specific mission application. The structural generalised use case compared constructing and using solid foams for a structural beam with constructing and using stainless steel and PEEK beams using a direct energy deposition process and a fused filament fabrication process, respectively. It was found that, while the solid foam beam required more volume than the other beams, it could be produced with significantly less energy and over a much shorter time span. The generalised thermal use case compared the construction and use of a solid foam insulator with a multi-layer insulator made of a PEEK frame and aluminium film, constructed using a fused filament fabrication and a physical vapour deposition process. It was found that, while a large mass of foam was required to produce that insulating layer, when compared to the multi-layer system, the foam layer took less energy to produce. The specific use case considered an aerocapture around Mars, in which solid foam was used to construct an aeroshell. This solid foam aeroshell was compared with an inflatable system and a chemical propulsion system to understand if it could provide a reduction in the proportion of mission mass required for the aerocapture. It was found that, for lighter missions a foam aeroshell could be used in a similar fashion to the inflatable system, however, it was noted, that the heat flux on the aeroshell would be significant, and further development would be needed to understand to protect the foam system form this high heat flux.

The thesis presents a plan for the future development of this research with a focus on verifying the material properties that a solid foam, produced in space, would have and developing a system capable of producing solid foams in vacuum and in microgravity. Two lines of enquiry are

proposed, a practical experimental enquiry and computational analysis. The results of either enquiry could be used to further the understanding of solid foams made in space and which applications they may provide an advantage too.

Acknowledgements

I would like to acknowledge the hard work and support of my thesis supervisor, Colin McInnes. Colin has provided consistent guidance throughout both the research and write up phases of this thesis. As well as provide brilliant support and guidance for my academic work, Colin is brilliant to work with as he has always been respectful and patient with all his interactions. He is a fantastic role model as an academic and a professional.

I would further like to acknowledge the support of my academic advisors and collaborators that supported me while I worked on the research presented in the thesis. Primarily I would like to thank Gilles Bailet who provided academic supervision while I researched the work presented in this thesis. Gilles provided a wealth of understanding of the field or in-space manufacturing and a drive to advance this technology further. I would also like to thank Craig White who provided support and research for the study into a foam aeroshell for an aerocapture manoeuvre discussed in this thesis in chapter 5.

Outside of the academic support I would also like to acknowledge the support of my family and friends throughout the development or the work presented in the thesis and the write-up of the thesis itself. I would like to thank Malcolm McRobb my friend and former college that encouraged me to pursue this research. I would like to acknowledge my parents Brenda Hastie and Brian Hastie, for all their support and for helping me learn to read and write (in spite of dyslexia) and sharing with me a lifelong love of mathematics. I would like to thank my siblings Larissa, Madeleine, Catherine, Jacqueline, Paula, Liam, Robert, Padraig and Dominic for their personal support. I would like to thank my partner, Alissa Gutnikova, for her support and patience while I have been writing this thesis and for encouraging me to complete this work.

The work reported in this thesis was supporting by funding from the Department of Science, Innovation and Technology (DSIT) and the Royal Academy of Engineering under the Chair in Emerging Technologies programme, I am grateful for their support.

Contents

Table of Figures

Table of Tables

Nomenclature

Acronym	Meaning
2D	2-Dimensional
3D	3-Dimensional
AM	Additive Manufacturing
ASI	Italian Space Agency
ASTM	American Society for Testing and Materials
CAD	Computer Aided Design
C_d	Drag Coefficient
CNC	Computer Numerical Control
COTS	Components Off The Shelf
DED	Direct Energy Deposition
DSMC	Direct Simulation Monte Carlo
E	Elastic Modulus
ESA	European Space Agency
F	Force
FCC	Face-Centred Cubic
FEA	Finite Element Analysis
FFF	Fused Filament Fabrication
FOS	Factor Of Safety
G	Bulk Modulus
G_C	Universal Gravitational Constant
H	Beam Width

HIAD	Hypersonic Inflatable Aerodynamic Decelerator
I	Second Moment of Area
IAC	International Astronautical Congress
IOM	In-Orbit Manufacturing
IR	Infra Red
ISM	In-Space Manufacturing
I_{sp}	Specific Impulse
ISRU	In-Space Situ Resource Utilisation
ISS	International Space Station
JAXA	Japan Aerospace Exploration Agency
k	Thermal Conductivity
L	Beam Length
LEO	Low Earth Orbit
M	Mass
MLI	Multi-Layer Insulation
Mo	Bending Moment
NASA	National Aeronautics and Space Administration
OGM	On-Ground Manufacturing
P	Pressure
PEEK	Polyetheretherketone
PLA	Polylactic Acid
PUF	Polyurethan Foam
PV	Photovoltaic
SBC	Stefan-Boltzmann Constant

SM	Subtractive Manufacturing
SOFI	Spray-On Foam Insulation
UV	Ultra-Violet Radiation
y	Distance from the Neutral Axis of Bending
β	Ballistic Coefficient
γ	Flight Path Angle
ε	Surface Emissivity
ν	Poisson's ratio
ρ	Density
σ	Mechanical Stress
σ_{Max}	Maximum Tensile Stress
τ	Shear Stress
Φ	Proportion of Material in the Edge of a Foam Cell Verse the Wall

1. Introduction

The aim of this thesis is to investigate novel technologies that could be used to fabricate devices in space. The research work reported in the thesis was inspired by the growing need for larger scale and more complex structures in space and the fundamental limitations of the current approaches to providing those structures. Currently, any structure used in space must first be manufactured on the ground, transported into orbit in a launch vehicle and then deployed and/or assembled in-orbit [1]. This thesis will consider the current state of in-space manufacturing, and which technologies could enable large scale in-space manufacturing. This research focused on the use of solid foams in the space and considered possible applications in detail.

1.1 The Demand for Large Scale Space Structures

The complexity and duration of space missions has increased over the past six decades and this trend looks likely to continue with the development of more complex missions such as the NASA Artemis moon exploration missions [2] or proposed asteroid mining missions by various private companies (for example the Asteroid Minning Corporation [3]). More infrastructure will be required in space to deliver these more complex missions, which will require ever larger qualities of materials, larger physical structures and increased power consumption. Such complex missions may require greater surface area, both to generate power for applications via photovoltaic solar arrays and dissipate waste power via radiation. This larger area would require larger structures. Larger structures could also be used for shielding of delicate components of habitats; storage for increased qualities of consumables or increased areas for solar sails.

In this thesis both large scale and macro scale refer to structures that are greater than 100 m in maximum length. This threshold has been selected as it is greater than the largest human made structures in-orbit, at the time of writing, such as the International Space Station (ISS) [4] and so would constitute a new capability for human made structures in orbit.

1.2 Current Limits of In-Space Devices

Most technologies that have been used, or are currently in use in space, have been constructed on the ground and then transported to space. This current manufacturing approach imposes several design constraints on large scale space structures:

- These structures must be able to support their own weight during their initial on the ground fabrication.
- These structures must be manufactured in a contaminant free environment to remove the risk of foreign objects before launch (an example of which is outlined in the ECSS's ECSS-Q-ST-70-01C [5]);

- To ensure the reliability of deployable mechanisms, extensive testing is often needed on the ground.
- The upper limit of the size of a structure is limited to that of the payload faring and structures often have to incorporate deployable mechanisms.
- The process of testing and transporting structures into orbit incurs significant mechanical loading on the structure and any on-ground manufactured structure must be designed to survive this loading.
- Any on-ground performance testing may not be able to recreate the space environment and the ability to correct or modify hardware after being delivered to orbit can be very limited.

1.3 Opportunity Presented by In-Space Manufacturing

In-orbit manufacturing could overcome many of the limitations that prevent current in-space devices form deploying large-scale structures and therefore enabling more complex space infrastructure and missions. Currently for a device to be used in space, it must be manufactured on the ground, stowed in a launcher's payload faring, launched and then deployed. As discussed above, each of these stages puts limitations on the design and development of that device. One of these limitations is size – currently any unit used in space must be stowed in the launcher's fairing and then deployed to its final shape. This process often involves complex mechanisms. A structure made in space would not have to deploy or be assembled, and so its final shape could be significantly larger than a traditional deployable structure. This is the one of the drivers behind the NASA OSAM-2 mission, which illustrates the potentially large scale of a structure made in space [6].

Space devices that are made on the ground must be made under their own weight in gravity and so must support their own weight at all points of the mission before the device reaches orbit. A device made in-space would not have this same limitation as its structure could be formed in microgravity. This would allow the device to be more mass efficient, as material would not be needed to support the mass of the device under loads due to gravity. This could mean that, for the same mass, the device could be substantially larger and capable of utilising a larger surface area for mission applications.

In-space manufacturing could remove many of the quality and verification requirements currently needed for devices made on the ground, as the device would be made in-situ in the space environment. Components made outside of an atmosphere, carrying dust and other materials, could be made with little to no contamination and would inherently meet the cleanliness requirements needed for component made on the ground.

1.4 Nomenclature

There are many terms used in this report that relate to specific technical processes. This section will outline what these terms are and what they refer to. In-Space Manufacturing (ISM) refers to any manufacturing process that occurs outside of the atmosphere of a planet. In-Orbit Manufacturing

(IOM) is a specific case of ISM that takes place in Earth's orbit. On-Ground Manufacturing (OGM) refers to all manufacturing processes carried out on the ground and transported to orbit for use there. In-Space Resource Utilisation (ISRU) is the use of resources found in-space for fabrication; this is as opposed to resources that are provided from the ground via a launch vehicle.

Additive Manufacturing (AM) can be described as the process of constructing a component by joining materials, this is similar to the description provided by Molitch-Hou et al [7] and the American Society for Testing and Materials (ASTM) definition, as described by Thompson et al [8] and Frazier [9] in their papers reviewing this topic. Additive manufacturing contrasts with Subtractive Manufacturing (SM), in which material is removed to form a 3D part.

1.5 Thesis Structure

This thesis contains six chapters:

1. Introduction – The motivation for the research, introduction to the core concepts and layout of the structure of the thesis.
2. Literature Review – An exploration of the research already conducted in the field and an examination of the areas for further development.
3. Trade Offs – An exploration of the key characteristics of an ISM system and comparison of these characteristics across a range of potential use cases.
4. Solid Foams in Comparable Use Cases – An exploration of the use of solid foams for ISM and comparison with other ISM processes in comparable use cases. This exploration considers the use of solid foams for ISM in general across a range of applications. The results shown in this chapter were reported in a paper presented by Hastie et al [10] at the 72nd International Astronautical Congress (IAC).
5. Solid Foams for Aerocapture Around Mars – An exploration of the use of solid foams, constructed using ISM, in more depth than the cases presented in chapter 4. This exploration considers the use of solid foams for ISM in a specific use case for one application. The results shown in this chapter were reported in a paper presented by Hastie et al [11] at the 18th International Planetary Probe Workshop.
6. Conclusions and Future Work – A discussion on future work that could be considered to further this research, as well as a summary of the thesis and its outcomes.

1.6 Published Works

The research presented in this thesis produced the results published in the following papers:

- Hastie, P. G.B., Bailet, G. and McInnes, C. R. (2022) On-Orbit Manufacturing of Large Space Structures Using Solid Foams. In: 72nd International Astronautical Congress (IAC), Dubai, United Arab Emirates, 25-29 Oct 2021, pp. 81-90. ISBN 9781713843085. This paper is discussed in chapter 4.

- Hastie, P. G.B., Bailet, G., White, C. and McInnes, C. R. (2021) The Use of In-Space Manufactured Solid Foams for Aerocapture. 18th International Planetary Probe Workshop, June-August 2021. This paper is discussed in chapter 5. The DSMC results presented both in the poster and later in this thesis are the work of Craig White, University of Glasgow.

2. Literature Review

2.1 In-Orbit Manufacturing

IOM is a special case of ISM that is carried out in orbit around the Earth. In the literature the terms in-orbit and on-orbit as well as fabrication and manufacturing, are normally used interchangeably to describe this process. For example, Boyd et al [1] use the terms "on-orbit" and "in-orbit" to describe the same process. This section will discuss the challenges of manufacturing in the in-orbit environment, the development of IOM technologies, the use cases and opportunities for this technology, the current state and scope of IOM research and important operational parameters for on-orbit manufacturing processes.

In-Orbit Manufacturing Challenges

The in-orbit environment presents many challenges for manufacturing and fabrication. The ultra-high vacuum and micro-gravity environment found in-orbit is a challenge for any space-based engineering activity [12]. As such, much of the investigation into ISM has focused on overcoming these challenges. For example, Lippman et al considered a thin film fabrication process that operated in a vacuum [13] and Prater et al considered AM in micro-gravity [14].

While the vacuum and micro-gravity requirements are significant, there are other challenges to manufacturing in orbit. Any autonomous IOM process will be remote, and access to instrumentation to monitor IOM could be limited. As discussed by Alexander et al [15], payloads for use in-space have to be designed with data storage and telemetry in mind. An IOM process may require an autonomous error detection and management process to ensure their correct functioning even whilst operating remotely.

Similar to other space missions, an IOM process would have to maintain a thermal balance in a temperature range that will not damage the mission hardware. This can be difficult in an orbital environment, in which there is variable solar input radiation (due to eclipses) , and the only means of dispersing heat is via radiation [6]. IOM presents an additional problem as many promising manufacturing processes, such as Fused Deposition Modelling (FDM) and Directed Energy Deposition (DED), require the feedstock to be heated to their melting point (up to 400°C) and so generate a large quantity of heat [7]. In some cases, there may be a requirement to remove heat rapidly to ensure manufacturing accuracy, so rapid heat dispersal is an additional challenge to consider.

As well as the thermal control requirements, there is also the challenge to generate power for these processes. Many fabrication processes are highly energy intensive, therefore any mission that incorporates an IOM process would have to provide sufficient power throughout its operational lifetime. Frazier et al [9] provides an overview of common metal AM process power requirements ranging from 100 W to 60 kW. This is a broad range, the in-operation value will be very dependent on the final process used. Patel [16] suggests a power to weight ratio for a solar PV array in space

of around 5-10 W/kg, a continuous IOM process that requires 100 W could require PV arrays as large as 10 kg in mass.

As was noted in the introduction, IOM removes some of the design constrains that limit traditional in-space hardware. It is important to remember, however that hardware manufactured using IOM will still be subjected to several environmental factors such as atomic oxygen erosion, ultraviolet degradation and cyclical thermal loads [12]. This must be considered in both the design of the final hardware and in the capability of the in-orbit manufacturing technology used.

In-Orbit Manufacturing Development

The idea of moving manufacturing processes for space applications into orbit has existed for some time. The first efforts to carry out manufacturing processes in space occurred in the 1960s and 1970s by both the Soviet space program and NASA. Notable examples from this period are the Soyuz 6 mission in 1969, in which welding was attempted in-orbit [17], the 1973 Skylab Brazing Experiments [18] and the Astor research corporation study into "in-space fabrication of thin-films" in 1972 [13]. Since the late 1990s there has been a push by both state funded space programmes and private institutions to develop IOM technologies with a specific focus on the development AM technologies. This has been described as a "Second Wave" of research on IOM by Skomorohov et al [19]. In 2014 NASA successfully operated a Fused Filament Fabrication (FFF) 3D printer, developed by Made In Space, on board the International Space Station (ISS) as part of their In-Space Manufacturing (ISM) project [14]. This marks a significant milestone in the development of in-orbit manufacturing. This was followed by ESA and ASI's POP3D (Portable On-Board Printer) mission which similarly demonstrated FFF printing in-orbit [20]. An image of the 3D printer on the ISS is shown in Figure 2-1.

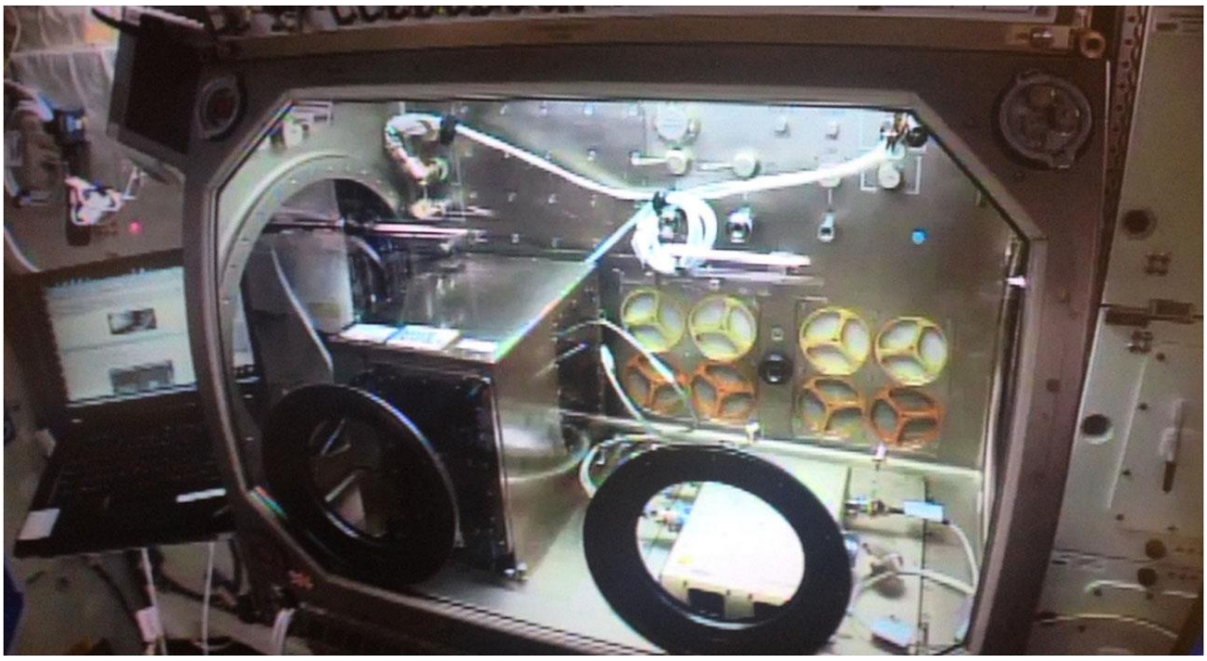

Figure 2-1 – Made In Space's 3D printer on-board the ISS. This image is from Prater et al [14] used with permission

As well as research into AM in micro-gravity, there has also been some research into AM in vacuum. Slejko et al used a modified commercial 3D printer to demonstrate 3D printing in vacuum using PLA with various filler materials [21]. While it is not explicitly stated it appears that this test was conducted on the ground and not under micro-gravity as there is not a discussion of set up of the test in orbit or control samples created on the ground. A vacuum chamber was used to simulate a low-pressure environment (10 Pa) similar to that found on-orbit. The The filler materials were selected based on their availability in space. To dissipate the heat generated by the 3D printer's hot end without convection, additional conductive pathways were connected to the printer. Samples printed in vacuum conditions showed similar mechanical and thermal properties as the control samples printed at atmospheric pressure. It was noted that the vacuum printed parts were slightly wider than the atmospheric pressure control prints. It is speculated that this increase in width was due to the reduction in surface tension of the 3D print stands. It was noted in the paper the pressure was 10^{-4} bar, which is significantly higher than the pressure observed outside of the Earth's atmosphere. This study appears to be the only fully reported example of 3D printing or AM conducted in vacuum and hence provides a useful proof of concept for 3D printing as an ISM technology. As is noted by the authors, the limitation of the pressure environment means that the results do not perfectly reflect the in-space environment and, as such, there may be further limitations placed on 3D printing in such environments.

Currently, there are several state and private entities developing technologies for IOM. Key players include:

- NASA's ISM project: Since 2014 they have now installed an Additive Manufacturing Facility (AMF) on the ISS and are working on adding a recycling process [22].
- ESA and ASI's POP3D which flew on the ISS in 2015.
- Made In-Space (now owned by Redwire) are continuing to develop in-orbit AM for the ISS. They currently have a number of projects in development considering diversifying the materials that can be printed and working towards their OSAM-2 mission (previously called Archinaut One), which aims to manufacture 10 m long beams in-orbit [6], [23]. Redwire reported that they demonstrated 3D printing in a vacuum in 2017 [6]. The OSAM-2 mission would demonstrate AM in vacuum and microgravity.
- Tethers Unlimited are working towards launching the SpiderFab satellite that will demonstrate IOM and assembly [24].

To date there has not been any demonstration of AM that is in-orbit outside of a pressurised container.

In-Orbit Applications

The field of IOM is broad and encompasses a large number of diverse manufacturing technologies. Because of this, in-orbit manufacturing has been suggested for use in a large variety of applications. In this thesis, the focus will be on the use of IOM to enable applications where it would not be

possible or practical to do so with conventional deployable structures. There are some common themes among the applications suggested:

- Macro-Scale: IOM could enable larger scale structures than conventional deployable structures. As discussed in chapter 1 section 1, the largest human made objects in orbit have a span of 100 m, these macro-scale structures could be larger than 100 m. Examples of potential macro-scale applications for IOM are described by McInnes et al [25] to build a reflector to harvest an M-type asteroid and Fraas [26] where IOM could be employed to construct the large scale mirrors were suggested.
- Adaptability: The ability to change the geometry of a structure or component in-orbit would provide new opportunities. This also enables recycling and repairing during the mission. An example of this is described by Lippman [13]. They suggest that the material used to construct thin-film sheets could be constructed from recycled parts that are no-longer in use. An example of adaptability of IOM is discussed by Wong et al [27] to create surgical tools during long duration missions.
- Material quality: The on-orbit environment provides a manufacturing location in hard vacuum and micro gravity; this means that products made on-orbit can be manufactured without defects caused by exposure to the atmosphere or significant loading under gravity. This is exemplified by Made In-Space's MIS Fiber [28] fabricator that used the micro-gravity environment to enable high quality fibreoptic manufacturing.

2.2 Thin-Film Physical Vapour Deposition

There are a number of vapour deposition processes that can be used to produce thin-films both as coatings and sheets. Vapour deposition processes are broken into two categories: Physical Vapour Deposition (PVD) and Chemical Vapour Deposition (CVD). Many vapour deposition processes require a vacuum environment and so they have been suggested for IOM [13]. This section will discuss Physical Vapour Deposition processes that may be useful in in-orbit manufacturing and discuss how vapour deposition could be used in specific applications on-orbit.

Physical Vapour Deposition Processes

A PVD process transfers material from a target feedstock to a substrate [29]. This is achieved by dislodging material from the target and directing it toward the substrate. The directing of this process is achieved by providing a large electrical potential between the target and substrate.

Material can be dislodged from the target by using a sputter or evaporation process. In the sputter process, material is dislodged by bombarding the surface of the target using ionised gas. This process frees particles as small as individual atoms from the target material, which are then free to travel through a vacuum to the substrate [29].

In an evaporation process, material is dislodged from the target by heating the target until it evaporates. The material is then free to travel across the vacuum to the substrate [29].

Sputtering can be achieved at lower temperatures than evaporation. For this reason, sputtering typically provides higher material densification on the substrate. Evaporation processes typically have higher deposition rates [29].

Physical Vapour Deposition In-orbit

PVD was suggested for use in-orbit by Lippman [13]. In this paper an evaporation PVD process is used to produce free standing thin-film sheets. It was suggested that this process could be used to make extremely thin-films of metal that could be used to fabricate a spin stabilised solar sail.

This process highlights a few of the key advantages of in-orbit manufacturing. The paper suggests the film feedstock could be recycled from material no longer required for the mission. This concept takes advantage of the adaptability of in-orbit manufacturing. The paper describes how the process could be used to produce thin-films that do not have a backing material. Backing material is required to spool and transport thin-films on the ground. These backing films add weight and increase the film areal density which is critical for solar sailing applications.

The problem of sheet/substrate parting is discussed in the paper. They described the problem of cracks in the sheet during extraction [13]. Further development of this PVD process could investigate ways to consistently extract the sheets.

2.3 Solid foams

Solid foams are a type of cellular solid. Cellular solids are solid materials that are filled with cells of enclosed space [30]. This basic definition covers a large range of materials, including honeycomb panels and wood. This section of the review will focus on solid foams. Foams have regular cells that repeat in 3D space and so can be described as providing a uniformed meso-structure. This uniformed meso-structure allows foams to provide somewhat consistent material properties over an extended envelope due to the addition of cells to the volume occupied. For this reason, foams are used extensively in applications that require low density components. The low density of foams is appealing for in-orbit manufacturing, as it means foams may have a high packing ratio of raw material to final structure volume. As will be discussed, the meso-structure of foams provides additional advantageous properties.

Solid Foam Fabrication

There are multiple ways to form a solid foam. A number of examples of processes for solid foam fabrication are described by Gibson et al [30] and Ashby et al [31] which focuses on metal solid foams. Most solid foams are formed using the following steps:

1. Foaming: The structure is formed while the material is in a liquid state.
2. Solidification: The material is solidified to hold the foam structure.

Foam formation is typically achieved by mixing gas into a liquid. As there is surface tension acting on the boundary between the liquid and gas, the gas in the mixture will form into cells where the outward gas pressure is balanced by the force of surface tension on the liquid boundary. From a kinematic point of view, the most energy efficient structure of a liquid with gas cells is that where the surface tension energy is minimised. As surface tension energy is dependent on the surface area, foam structures tend to organise toward minimum surface area formations. A comprehensive review of the process of liquid foam formations is provided by Drenckhan and Hutzler [32]. In this paper Drenckhan and Hutzler examine the physical structure of foams. In-particular, they place importance on a foam's liquid fraction – the volumetric proportion of the foam that is made of liquid, and the polydispersity – the variation in cell size across the sample. The effects of these properties are well illustrated in their paper and shown here in Figure 2-2 below. The structural arrangements of liquid foams can be divided into two categories: dry and wet. A dry foam has a low liquid fraction, and so the most efficient packing arrangement for the foam structure is a thin-film foam with boundaries that follow Plateau's laws [33] that is: each cell is bounded by thin-film walls, 3 cell walls meet to form a vertex and vertexes meet in nodes of 4. In wet foams gas cells are spherical and stack in the most volumetrically dense manner that can be achieved, this is typically a Face Centre Cuboid (FCC) arrangement.

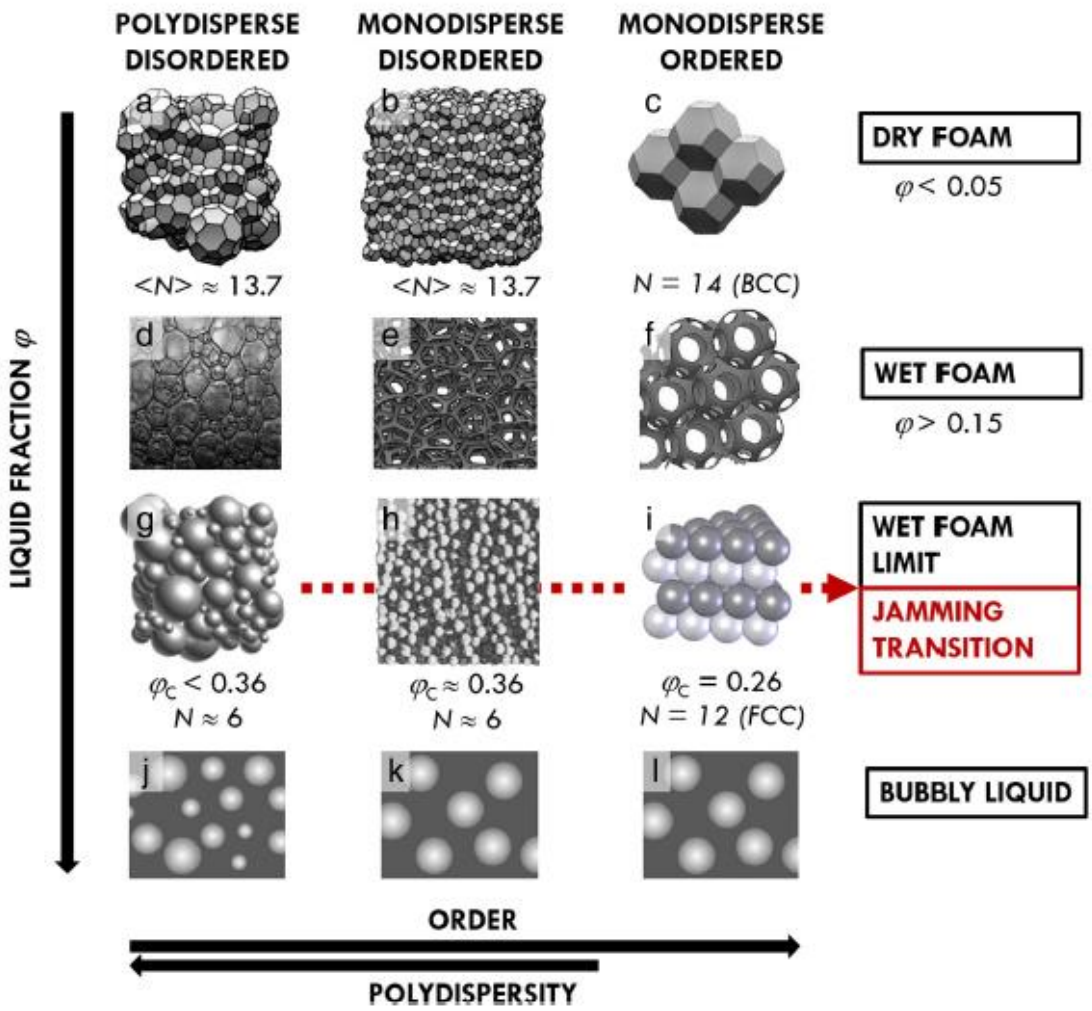

Figure 2-2 – Foam Structures dependent on liquid fraction and polydispersity [32] used with permission

Gas is typically introduced into foams one of two ways:

1. Chemical reactions: The gas in the foam is released due to a chemical reaction that takes place during formation. Examples of this include polyurethane foams and cellular concrete [34]
2. Blown foam: The gas is pumped into the liquid and mixed. This is the foaming process employed in foam soap dispensers, as well as melt gas injection metal foams [31].

Chemical reactive gas release is often caused by reagent mixing, as was the case for the polyurethane foam developed for the proposed REDEMPTION mission [35]. There are also examples of reactions being triggered by environmental stimulus, such as the case for the foam produced by Schlögl et al [36]. In this paper the gas was produced as a product of a reaction triggered by UV radiation.

Blown foams often use a gas injection process, such as that used in Hydro or Cymat aluminium [37], or blown over wet meshes as is seen in soap foam dispensers.

There are several solidification processes that have been used to solidify foams. Two prominent methods are cooling and chemical structural change brought on by reaction. Cooling is often used in metal foam production [31]. Numerous plastic foams change their chemical structure by introducing cross links between polymer chains and causing rigidification. These rigidification processes a typically triggered by the introduction of reagent or exposure to activating radiation such as UV light. The polyurethane foam used by the REDEMPTION mission [35] was rigidised due to the introduction of a reagent, in the same manner as gas production. UV curing was carried out on the foam produced by Schlögl et al [36].

The quality of the meso-structure in solid foams that are produced using chemical reagent mixing is heavily dependent on the chemical composition and qualities of those reagents in the reaction. Valdatta et al [35] describes that, on the REDEMPTION mission, the chemical formulation used for the polyurethane production had to be adjusted to change the pressure of gas produced in the foaming step. A blown foaming process may provide more control over gas injection and thus the foam meso-structure.

There are some noticeable exceptions to this two-stage solid foam production model. Some metal foams are formed by casting over moulds [31] , which are then removed. Some foams are produced via sintering of hollow spheres, which is the case for polystyrene and some metal foams [31].

Solid Foam Material Properties

The nature of 3D repeating cellular structures changes the bulk material properties of foam. As the use of engineered foams has increased in the past 50 years, there has been a corresponding increase in research into the material properties of these solid foams. One of the most frequently cited sources in the literature on the properties of foams is the book by Gibson et al [30]. In this book Gibson et al provide a number of methods to derive foam properties form the quality of the foam and the solid base material in the foam.

On the mechanical properties, Gibson et al suggest what is often described in later research as the Gibson-Ashby model. In this model the foam consists of cuboid cells joined together in a repeating 3D pattern, an image of which is shown in Figure 2-3. A series of equations to estimate the mechanical performance of foams can be derived from the Gibson-Ashby model. These equations are dependent on whether the foam has an open or a closed cell structure, if the cells of the foam are open or closed to each other. A closed cell foam has an additional mechanical strength from the walls of the cell and the gas pressure in the cell. Some of the results provided by the Gibson-Ashby model are shown in Table 2-1.

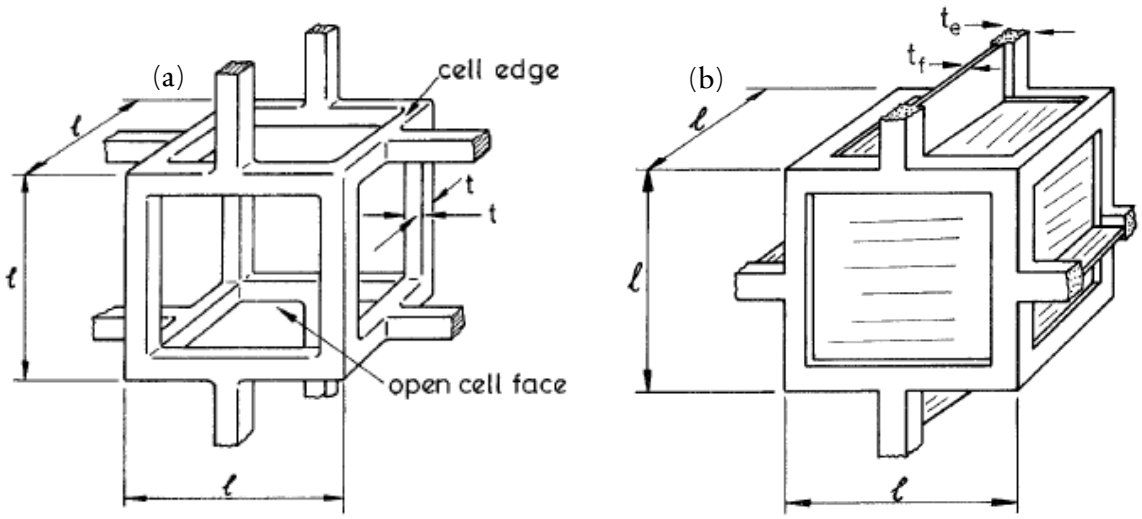

Figure 2-3 – The Gibson-Ashby cubic model. (a) Open-cell model (b) Close-cell model [30] used with permission

Table 2-1 – Gibson-Ashby equations for foam mechanical properties adapted from [30]

Mechanical Property	Open Cell	Closed Cell
Elastic Modulus	$\frac{E_{Foam}}{E_{Solid}} \approx \left(\frac{\rho_{Foam}}{\rho_{Solid}}\right)^2$	$\frac{E_{Foam}}{E_{Solid}} \approx \left(\phi\frac{\rho_{Foam}}{\rho_{Solid}}\right)^2 + (1-\phi)\frac{\rho_{Foam}}{\rho_{Solid}} + \frac{\rho_{Gas}(1-2\nu)}{E_{Solid}\left(1-\frac{\rho_{Foam}}{\rho_{Solid}}\right)}$
Bulk Modulus	$\frac{E_{Foam}}{E_{Solid}} \approx \frac{3}{8}\left(\frac{\rho_{Foam}}{\rho_{Solid}}\right)^2$	$\frac{E_{Foam}}{E_{Solid}} \approx \frac{3}{8}\left\{\left(\phi\frac{\rho_{Foam}}{\rho_{Solid}}\right)^2 + (1-\phi)\frac{\rho_{Foam}}{\rho_{Solid}}\right\}$
Compression Strength Plastic material	$\frac{\sigma_{Foam}}{\sigma_{Solid}} \approx 0.3\left(\frac{\rho_{Foam}}{\rho_{Solid}}\right)^{3/2}$	$\frac{\sigma_{Foam}}{\sigma_{Solid}} \approx 0.3\left(\phi\frac{\rho_{Foam}}{\rho_{Solid}}\right)^{\frac{3}{2}} + 0.4(1-\phi)\frac{\rho_{Foam}}{\rho_{Solid}} + \frac{p_{Gas}-p_{Atm}}{\sigma_{Solid}}$

Here, ϕ is the proportion of material in the edge of the cell verses the wall, σ is the stress, E is the elastic modulus, G is the bulk modulus, P is the absolute pressure, ρ is density and ν is Poisson's ratio.

As can be seen from Table 2-1, the reduction in the elastic modulus of a foam, compared to its solid material, is directly proportional to the square of the solid material fraction (ρ_{Foam}/ρ_{Solid}), which has significant implications. The foam solid material fraction is inversely proportional to the increase in the foam volume, when compared to a solid part with the same mass. For a beam this would mean the thickness of the beam would increase inversely to the foam solid fraction, and so the second moment of area of the bean would increase inversely to the cube of the solid fraction. Hence, a foam beam would be likely to have a greater flexural rigidity than a solid equivalent with the same mass width and length.

The Gibson-Ashby model is widely used to estimate the mechanical properties of foams. However, Fischer et al reported that it did not accurately describe the recorded properties of polyvinylchloride (PVC) foams [38]. Fischer et al developed an FEA model to simulate the mechanical properties of

PVC foams more accurately. A summary of this accuracy is illustrated in Figure 2-4 which has been sourced from Fischer et al.

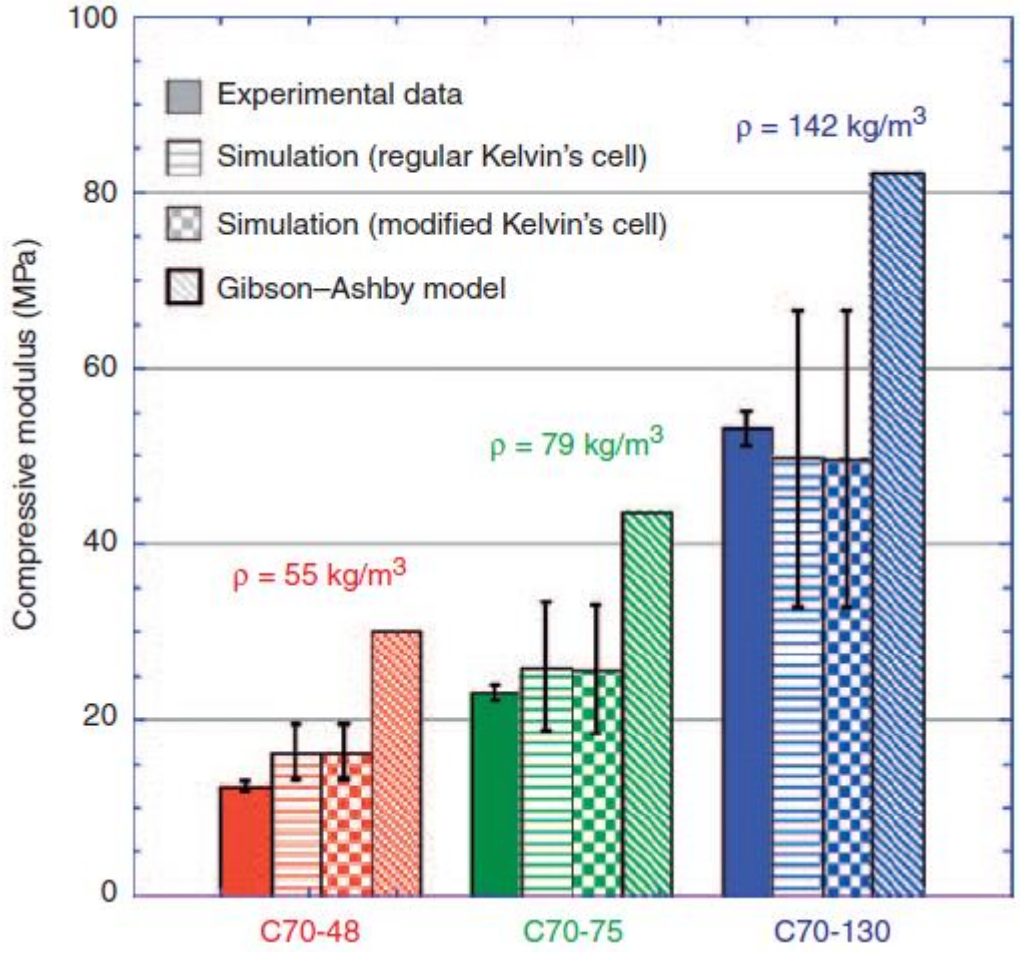

Figure 2-4 – Comparison between Gibson-Ashby model and the FEA carried out by Fischer et al. [38] used with permission

Gibson et al [30] also provide models for foam thermal properties. They describe how the thermal conductivity of the foam can be found by summing the thermal conductivity of the foam component parts. The foam component thermal conductivities are:

- Conduction through the solid material. This can be estimated as the product of the solid material thermal conductivity, the solid fraction (ρ_{Foam}/ρ_{Solid}) and an efficiency factor.
- Conductivity through the gas in the cell. This can be estimated as the product of the gas material thermal conductivity and the gas fraction ($1-\rho_{Foam}/\rho_{Solid}$)
- Convection across the cell. Typically, the cells of a foam have a low Grashof number, due to their small size and so experience little to no convection across the cell.
- Radiation between the faces of the cell.

Typically, the thermal conductivity of a foam is much smaller than that of the constituent solid material.

Feasibility of Solid Foam Structures in-orbit

As discussed in section 2.1, the feasibility of a process for IOM can be evaluated by asking if the process can operate in both a vacuum and micro-gravity. There are examples of foams forming in these environments. As discussed previously, the REDEMPTION mission [35] used a modified formulation of reagent to form a polyurethane foam in vacuum. The modification carried out on the foam showed the importance of lowering the gas injection pressure in vacuum. Unfortunately, a technical problem with the mission meant that the payload was not deployed during the rocket launch, so there is no micro-gravity data from this mission.

Several foam studies have been carried out in micro-gravity environments, this includes: studies by Garcia-Moreno et al on X-Ray radioscopy of liquid metal foams [39], Quadrini et al on solid-state foaming of epoxy resin [40], Langevin et al on aqueous wet foams [41] and Somosvári et al on foam evolution and stability through the FOCUS experiment [42]. The FOCUS experiments carried out by Somosvári et al studied the development of foams on the ISS and so provides an example of foam research in micro-gravity. FOCUS found that micro gravity bubbles were slightly larger than their terrestrial counterparts but had similar longevities. It would therefore appear that solid foam production may be possible in-orbit.

2.4 In-Situ Resource Utilisation

An important advance in the field of in-orbit manufacturing is the development of technologies to enable the use of material in space as feedstock. The use of in-situ resources would mean that, structures made in-orbit, could be independent of material launched on the mission. This has been described as In-Space Resource Utilisation (ISRU) [43].

ISRU has been suggested for use with numerous different sources of material including:

- Asteroids as discussed by McInnes [25]
- The moon as discussed by Gerdes et al [43] or S. L. Taylor et al [44].
- On Mars as discussed by Buchner et al [45]
- Reusing discarded mission components as suggested by Lippman [13] or Mariappan et al [46]

Research has been conducted to demonstrate the utilisation of space-based ISRU. A study conducted by Lietaert et al [47] demonstrated ISRU by using meteorite material, as the feedstock, to a laser Powder Bed Fusion (PBF) process. The study found that the meteorite material was able to be used in a PBF process. This is significant because this is the first-time parts have been made using meteorite material in a metal AM process. The study found that parts produced using this meteorite material had some material defects – low relative density and cracks. These defects may suggest the parts have poorer mechanical properties when compared to their terrestrial source counterparts, however no mechanical testing was reported in this paper. The material used was pre-processed into powder using gas atomisation. A fully realised ISRU process will have to develop technologies to undertake any pre-processing in-orbit.

A study conducted by Buchner et al [45] used simulated Martian regolith as a feedstock for an Additive Manufacturing (AM) process. This process produced cement from Martian regolith and phosphoric acid. The cement was layered using an additive manufacturing process, which used a CNC gantry. The study demonstrated the building of a small shelter-like construction. Mechanical tests showed that the cement produced by the process had a similar compressive strength to terrestrial cement. The test was conducted in laboratory conditions. While the fact that this study does not demonstrate a build process outside of the atmosphere of a planet makes it less applicable to ISM, it does demonstrate the use of an autonomous build process using in-situ resource, something that would be key to future ISRU.

As well as exploiting natural space resources, such as meteorite material or lunar regolith, there is also active research into the utilisation or recycling of terrestrial sources of material already in-space. It is suggested by Lippman [13] that the feedstock for a PVD produced thin film process could be provided by components that are "no-longer needed for the mission". More recently Mariappan et al [46] describes a recycling process design to utilise captured space debris. In this study, Mariappan et al propose a novel recycling process converting captured space debris into aluminium powder, silicon powder and water vapour. The study's intention is to use the aluminium powder for propellant, the silicon for soil and the water vapour for orbital manoeuvring. As well as the application stated by the author, it appears that materials like silicon and aluminium powder could be used for creation for structural and electrical devices using in-space manufacturing.

2.5 Literature Review Summary

A review of the literature has shown that, while there is currently a great deal of interest and significant milestones have been met, such as the construction of 3D printed tools in space [14], there are still significant limitations on what can be made using this technology and most examples found have been cited as technology demonstrations rather than a fully adopted technology. To date, there are no examples of a fully autonomous ISM facility that could be used to create a large space structure, as has been envisioned by the OSAM-2 mission [6]. There is a great deal of development planned for ISM, with a number of possible manufacturing processes and construction materials considered for this application. Solid foams have already been considered as a material that could be made in space in a limited application in the REDEMPTION mission.

There has been some research into the ISRU for ISM processes, and some on the ground demonstration of AM manufacturing using samples for space. However, no examples have been found that shows the use of material gathered in space and using processes that have been shown to be possible to carry out in orbit. There is a great deal of interest in ISRU for ISM, particularly for use in planetary and asteroid exploration.

There is an extensive literature on manufacturing of foams and the material properties of solid foam. While there has been a great deal research toward predicting material properties of foams based on its bulk material, it appears that final material properties can vary from commonly used models such as the Gibson-Ashby equations. For this reason, where possible, this thesis uses solid foam material properties that are based on reported empirical data. This is not possible for some of the novel materials discussed. It is important to note that, because the empirical data used for the

solid foam material properties is based on terrestrial data there may still be some variability in the final properties.

3. Trade Offs

As discussed in chapter 2, to date the only examples of IOM have been carried out in a pressurised environment on board the ISS [14]. This is a significant step forward in the development of IOM, however such in-atmosphere IOM would be limited to building structures inside a pressurised container and could not fully exploit the benefits presented by IOM. In particular such technologies could not be used to fulfil the macro-scale applications discussed by McInnes et al [25] or Frass [26]. To be able to construct a macro-scale in-orbit structure the manufacturing technology would have to demonstrate that it can operate autonomously in the space environment without a protective atmosphere around the build.

Therefore, there is still a gap in the technology available for IOM. As well as the requirement to operate in the space environment, there are other important characteristics that must be considered for the successful deployment of IOM technologies. These may include:

- Deployment/print time – The time it takes for the structure to be constructed, checked and commissioned.
- Autonomy – The capability of the technology to run without operator intervention, this includes all stages of the build, inspection and commissioning.
- Adaptability – The capability of the technology to be used for more than one purpose or to adapt to meet the mission requirement.
- Resource effectiveness – How effectively the technology can deploy the resource that it processes.
- Reliability – How reliable the technology is at producing hardware and how consistent the quality of that hardware is.
- Whether or not the technology can utilise in-space resources – Can the technology utilise materials found in space such as materials found on asteroids, extraterrestrial bodies or discarded mission equipment

3.1 Deployment Time

Traditionally, once a spacecraft is launched it must go through a process of commissioning before entering full operations [48], [49]. The construction of hardware using ISM would become part of the commissioning operations. Commissioning operations are generally non-productive towards the main mission objectives, hence shorter commissioning operations can lead to a reduction in unproductive time, increase the effective mission length and reduce mission overhead costs. For a mission using IOM, the deployment of hardware manufactured in orbit could take a significant proportion of time. This is of relevance to shorter missions such as CubeSat or Small Sat missions in LEO which may have a mission life that is less than 10 years [48]. For longer missions, such as

those outside of LEO or on interplanetary missions, a longer build process may be more acceptable, particularly that time would allow for the construction of a more capable structure.

Given that ISM could be used to produce a wide range of products the most effective metric to compare deployment effort could be the print rate – that is the rate at which an AM process makes useable material – as print rate will scale directly with deployment time, regardless of the specifics of the scale of the product being made. The print rate characteristic can be shown as a volume, area or mass rate, depending on the use case.

Print rates can be compared across a range of processes proposed for ISM. The material selected and the manufacturing process will affect the print rate of solid foam. This trade off will focus on the use of Polyurethane Foam (PUF) given that these foams have been considered for use in space [35]. To understand the parameters of a PUF AM process, the study of a 3D printing cable suspended robot presented by Barnett and Gosselin [50] was used as an example. This study was selected as it showed an example of a full 3D printing process using foam, and so shows a practical application of the process rather than a theoretical maximum case. The study presents a variable flow system with a peak material flow of 5 g/s. Given that the PUF used had a density of 25kg/m^3, the peak flow rate equates to a volumetric rate of 2x10^5 mm^3/s. The study also reports the total time – 38 hours – and volume – 298 L – for the print. This can be used to find estimates of the average volumetric and mass rate as 2178 mm^3/s and 0.054 g/s, respectively.

The volumetric print rate for of a Fused Filament Fabrication (FFF) process using PEEK is reported by Li and Lou [51], as part of a study into the tensile bending strength of 3D printed samples. The study reported a print rate of 30 mm/s, with a maximum nozzle size of 0.4 mm. If it is assumed that the nozzle is circular in shape, then the volumetric print rate $\dot{V}$ can be calculated using the diameter of the nozzle $\emptyset_N$ and the print rate v_{Pr} in the following equation.

$$\dot{V} = v_{pr}\,\pi\left(\frac{\emptyset}{2}\right)^2 \qquad 3\text{-}1$$

In equation 3-1, the volumetric print rate is the product of the cross-sectional area of the nozzle and the print rate (as reported by Li and Lou [51]). Assuming that the nozzle is circular, the cross-sectional area of the nozzle is the product of π and the square of half the nozzle diameter.

The volumetric printing rate reported would result in a volumetric print rate of 3.770 mm^3/s. This research was conducted using Apium PEEK 450, which the supplier reports [52] as having a density of 1.3 g/cm^3. The mass rate of this FFF process is the product of the volumetric print rate and the density which is 4.901x10^{-3} g/s.

In their research on the material properties of materials made using metal AM process – Direct Energy Deposition (DED) – Zhang et al [53] reported on the mass print rate of the process used. The rate varied with power consumption of the process, at low power (600W) the process was reported to having a flow rate of 4g of powder per minute or 6.667x10^{-2}g/s, at high power (1400W) the process was reported to having a flow rate of 20g of powder a minute 3.333x10^{-1}g/s. These process used Stainless Steel 316, which is reported to have a density of 8.00g/cm^3 by Yakout et al [54]. The density can be used to find the volumetric print rate of the low and high-power process of 8.333mm^3/s and 41.667mm^3/s, respectively.

Examples of the mass and volumetric print rates of an AM process using PUF, PEEK filament (using a FFF process) and Stainless Seel 316 (using a DED process) are shown in Table 3-1. Also shown in Table 3-1 is the time it would take to print a cubic meter with each of these approaches.

Table 3-1 – Print rates for various AM processes

Approach (Process and Material)	**Volumetric Print Rate $\dot{V}$ [mm³/s]**	**Mass Print Rate $\dot{M}$ [g/s]**	**Time Taken to Print a Cubic Meter [s]**
AM process, PUF	2178	0.054	4.591×10^{6} (2 weeks)
FFF, PEEK	3.770	4.901×10^{-3}	2.653×10^{9} (82 years)
DED (600W), SS316	8.333	0.067	1.200×10^{9} (38 years)
DED (1400W), SS316	41.667	0.333	2.400×10^{8} (8 years)

While the mass print rates of each of these processes are comparable, the volumetric flow rate of the PUF process is between two and three orders of magnitude greater than the DED or FFF process. It is possible that the print rates of the FFF and DED processes would increase in specific conditions, with specific material or with a second printer head, but these improvements would have to be substantial and could have knock on implications to other characteristics of the process.

3.2 Autonomy

The remote nature of satellite applications means that autonomy is an important consideration for any technology deployed in space. The extreme remoteness of a space platform makes it difficult for operators to accesses performance and intervene. Given that the products of an ISM process may require the control of multiple parameters for long durations of time in the extreme remoteness of space, the need for autonomy in ISM may be even greater than a conventional satellite application. Technologies used for ISM would have to consider how the materials produced are inspected and how errors can be corrected for.

The choice of ISM process could affect the complexity of the systems used to control the process and the ease with which an autonomous system could be developed or how robust that system would be. The more consistent and predictable an ISM process is the easier it will be to control and to develop a robust autonomous system. Additionally, processes which require fewer parameters to be monitored for a successful print may also be easier to automate, as fewer parameters will require fewer sensors. The ease of which a robust autonomous system can be developed for an ISM process is closely linked with the reliability of the process.

Given how critical the specifics of the system design would be to the autonomy of any ISM process, and how early the concepts of ISM process are, it is difficult to make a direct comparison between different ISM process beyond reinforcing the importance of process reliability

3.3 Adaptability

As discussed in chapter 1 section 3, an advantage for ISM is the ability to adapt to changing scenarios and mission objectives. Additionally, an ISM process that can be adapted for use across a range of applications may be able to spread its cost of development over more mission and customers, hence it is possible that an ISM process that is highly adaptable is also more economically viable.

One metric that could be used to compare the adaptability of ISM processes might be the number of use cases that a particular ISM process can be used to construct. For example, a FFF process, such as the one demonstrated on board the ISS discussed in [14], typically produces plastic components which might limit the possible application of this technology to purely structural components, without the ability to produce material that could be used for thermal or electronic components.

The PVD process (discussed in chapter 2 section 1) is used to make a wide range of products for on ground applications. The PVD process produces thin films [13] which are used for a great deal of applications. The PVD sputtering process is used in the construction of solar reflective material, as described by Mengali et al [55]. These solar reflectors are key components in satellite thermal management as they provide surfaces with a low solar absorptivity and high IR emissivity, which makes the surface more effective at emitting heat and less effective at absorbing heat from the environment [56]. The PVD processes are used in the manufacturing of a wide range of electronics including batteries, as described by Lobe et al [54]. PVD can also be used in the construction of optics including computer-generated holograms, as discussed by Zhang et al [57]. As discussed chapter 2 section 2, Lippman suggests using PVD to produce solar sails [13] which could be used for orbital manoeuvres. While PVD has been shown to be capable of making a wide range of products, both the process and the feedstock would have to be changed to produce some of these products. One PVD process may not be capable of producing all the product explored.

Solid foams (discussed in chapter 2 section 3) are used for many applications. Solid foams already see extensive use as insulating materials. PUFs have been applied to the cryogenic fuel tanks of launch vehicles [58] both in-atmosphere and in vacuum. Typically, this foam insulation is applied in the form of spray-on foam insultation (SOFI) that can be easily applied to large complex shapes – such as fuel tanks – or applied to multi-layer insulation (MLI) for use on deep space cryogenic tanks, as discussed by Xiaodai et al [59]. PUFs have been used in structural components such as roofing described as Keller et al [60], in which PUF was used as part of a sandwich board. In many cases, when PUFs are used for a terrestrial structural applications, they are reinforced with other materials to provide greater load bearing capacity. It is possible that in an orbital micro gravity environment that PUF may not need this support material.

3.4 Resource Effectiveness

Regardless of the technologies selected for an in-space manufacturing system the process will require the utilisation of resources. A system that can more effectively use resources to create

products will be able to create more produces for a given cost and reduce the amount of scrap or unused resources.

The resources needed for an in-space manufacturing system would include both feedstock and electrical power. In the case of feedstock, the expense of supplying this resource would include not only the typical extraction and refinement cost of a terrestrial manufacturing process, but also the cost to transport that material to orbit. Currently the price to deliver a kilogram of material to LEO can be estimated at $3170 (22,000 kg at $69.75 M) on a fully loaded Falcon 9 rocket [61]. In-space manufacturing systems would thus have an even greater cost for feedstock than a terrestrial system when the resource is supplied form a terrestrial source, and so the effectiveness of raw materials is of critical importance to an in-space manufacturing process. To compare the effectiveness of the feedstock utilisation to make a product, the comparative mass of the products, made using different processes could be used. For this comparison to be effective the product that is produced must have comparable functionality. As will be explored further in chapter 4 discussing solid foam use cases, a simple comparison between these different techniques can be found by using the example of a loaded beam as presented in Hastie et al [10]. This paper explored the difference in mass of a square cross-sectioned beam when loaded in bending with the same load at the same distance. The results of this study are shown in the table below:

Table 3-2 – Comparative mass of simple beams, presented in Hastie et al [10] table 1

	Foam	**FDM**	**DED**
Thickness (mm)	18.2	5.2	2.8
Beam Volume (m^3)	3.3×10^{-4}	2.7×10^{-5}	7.7×10^{-6}
Tensile Yield Strength (MPa)	1.99	87.34	558
Density (kg/m^3)	160	1300	7990
Beam Mass (g)	53.0	34.6	61.8

As is shown in Table 3-2, while the solid foam has a low density the volume required to support the load, using a simple square section, is much higher than the other manufacturing processes and so its overall mass and its resource efficiency is broadly comparable with the other manufacturing processes presented. Other functional comparisons are presented in Hastie et al [10] and will be discussed in detail later in chapter 4. While foams are mass/ resource efficient when considering purely the volume occupied, it is possible that other processes may be more efficient for products with specific functions.

Electrical power should also be considered a resource when considering the resource effectiveness of a manufacturing process. Satellites in Earth orbit are typically powered by solar arrays. A solar array's power generation scales with its surface area meaning that larger power demanding applications require large, heavy solar arrays to power them. A system that requires a large amount

of energy to create a product would require a large solar array to provide the power required or accept a prolonged deployment time if the power consumption can be throttled or cycled. As with the raw material cost, larger and heavier power generation equipment would increase the transportation cost to orbit, as well as the system hardware cost. In this case, a measurement of energy per effective unit of volume or energy per effective unit of area, would be useful to compare technologies depending on the application in use. For example, a complex 3D structure may be best to consider in terms of energy per unit of volume whereas a large planer structure, such as a solar array, could be better considered in terms of energy per unit of area. As with the feedstock resource effectiveness, it may be more useful to consider the energy consumption to produce comparably functional products. As will be discussed, this comparison was also considered in Hastie et al [10]. With an estimated foam power consumption of around 1/100 of the DED printing process and a shorter printing time, foam can be seen to have a much greater resource effectiveness than the other processes considered when considering the electrical power.

As an in-space manufacturing system would be physically isolated form the Earth, low resource effectiveness would also have a detrimental effect in the form of waste. Over time this could build up in the systems and lead to damage or cause space debris if not contained suitably. In the case of power generation, power that is generated but not used in the manufacturing process directly, due to inefficiency, may be dissipated as heat which would have to be managed within the in-space manufacturing system. The dispersal of this heat from the system would require additional thermal management systems which could add both mass and complexity to the system.

3.5 Reliability

Given the remote nature of space applications outside of the Earth's atmosphere, there is almost no opportunity for a user to manually correct faults or even detect faults. This limitation is a significant design driver for all space applications but may be particularly significant for an IOM facility. Not only must the manufacturing facility operate autonomously, but the products that the facility creates will go on to become critical components for other systems, many of which will be autonomous themselves. Hence, the reliability of an IOM facility can be considered on two levels:

- How consistent are its products – a quality of manufacturing question
- How consistently can it operate autonomously – an operational reliability question

This thesis uses the definition of reliability offered by Sun et al in Reliability Engineering [62] which is the "property of an object to maintain in time, within the established limits, all parameters that ensure the performance of the required functions in the specified operating conditions".

The reliability of the products produced by a facility can be considered by exploring the variability of the properties of these products when produced using terrestrial process. For example, to understand the repeatability and reliability of the strength of polyurethane the variability of strength in a polyurethane terrestrial polyurethan sample could be explored. As was discussed in the literature review, the properties of a solid foam are dependent on its mesostructured which can be influenced by variations in the manufacturing process as exemplified by the sample produced during the REDEMPTION mission [35].

Reliability of the facility as a system can be considered by exploring the likelihood of system failure over a given period. This can be explored by considering the time to failure of terrestrial applications or considering the complexity of the process. A comparison of the reliability of the process could be made by considering how widely adopted the technology is, in this regard processes such as FDM have been widely adopted and are available for general use.

3.6 Compatibility with ISRU

As discussed in chapter 2 section 4, a technology that can enable ISRU holds the potential of untying the manufacturing process form Earth-based support. As such, there may be many applications where the in-space manufacturing approach must be capable of ISRU, partially for long term, extremely large and deep space applications when support from the ground can be logistically challenging or even unfeasible. Technologies that are not capable of ISRU may still have extensive applications in space but may be limited. It may be possible to consider some ISRU capability if the technology is capable of recycling and reusing materials form either space debris or parts of the mission that are no longer needed, such as was suggested by Lippman [13].

Some of the technologies considered in this thesis have already been considered for ISRU. Alternatively, some of the technologies considered could not feasibly use in-situ materials as their process is dependent on materials that can be difficult to find out with Earth or the material quality and preprocessing requirements are such that it is not practical to use in-space resources. An example of this may be the complex hydrocarbon and organic chemistry required for polymer manufacturing. Even while some of the basic components of this stock material may exist outside of the Earth, such as the hydrocarbons found on Titan [63], the complex processes required to form the stock may be difficult to transfer to space. Prepossessing limitations on stock material is not limited to chemistry, it could also include material consistency, shape or even storage.

3.7 Comparison

A weighted table can now be used to compare the performance of the following processes.

- Direct Energy Deposition (DED) using a metal feedstock
- Fused Deposition Method (FDM) using polymer filaments
- Physical Vapour Deposition (PVD) using a metal feedstock
- Solid foam manufacturing

These processes shall be compared across three cases, in each case the weighting has been adjusted to account for the different needs for each use case. In each case the following parameters shall be considered:

- Deployment/print time – from 1 to 5, 5 being a short deployment time and 1 being a long deployment time

- Ease of automation – from 1 to 5, 5 being a process that would be easy to control remotely with an automated process and 1 being a process that would be challenging without an operator supporting the process
- Adaptability – from 1 to 5, 5 being a process that could be used to manufacture a range of products without hardware changes and 1 being a process that is only capable of manufacturing products used in one application
- Resource effectiveness – from 1 to 5, 5 being a highly efficient process and 1 being an inefficient process
- Reliability – from 1 to 5, 5 being a highly reliable process that produces products of a consistent quality and 1 being an unreliable process that produces poor quality products
- ISRU compatibility – 0 to 2, 2 being a process that could conceivably produce products from feedstock that is exclusively found in space and each stage of the process can be carried out on-orbit, 1 being a process for which a significant majority of the resources and each stage of the process can be carried out on obit, and 0 being a process where the majority of the resources must be produced on the ground and/ or one or more of the process stages can only be conducted on the ground

The use cases considered for this comparison have been selected to consider a range of possible applications that have been proposed for ISM. The cases are described below:

- Short term use case – In this case, ISM is used to adapt one satellite to enhance its capabilities, the ISM facility is not intended for use beyond the lifetime of this mission, and it is not intended for this ISM process to be resupplied. This use case is similar to Redwire's OSAM-2 mission [6], where the ISM facility is aimed at producing a truss for a solar array.
- Medium term use case – In this case, the ISM facility is designed to make products in space that will improve the capabilities of other satellites over its lifetime, it is intended that this facility will be re-supplied.
- Long term use case – In this case, the ISM facility is intended to construct larger infrastructure over a longer period to produce infrastructure that would not be possible to launch. An example of such a large-scale structure could be the large mirrors suggested by Fraas [26] and could extend to much larger structures in the future.

The estimated unweighted performance of each of the four methods is shown in Table 3-3 below. These performance scores were estimated by the author.

Table 3-3 – Unweighted comparison table

Process	DED	FDM	PVD	Solid Foams
Deployment Time	3	2	1	5
Ease of Automation	2	3	2	2
Adaptability	2	3	4	2
Resource Effectiveness	3	3	3	3
Reliability	3	4	3	2
ISRU compatibility	1	0	2	0
Total	14	15	15	14

The weightings used for the short-term case are listed from highest to lowest below:

- Deployment time: 2.5 – In the short-term mission the deployment time takes a considerable proportion of the overall mission time and so is a key consideration in this mission's comparison.
- Ease of automation: 2 – A system that is difficult to automate will take longer to commission and operate, this would take up a significant proportion of the mission lifetime.
- Resource effectiveness: 2 – In this case, the mission is not being resupplied and all material must be transported in the initial launch, additional resources could increase the mission mass or cut down on the mass of the payload to fit the requirements.
- Reliability: 2 – In the short-term case there is less time to compensate for unreliable products and so the quality of products made by the ISM facility should be high.
- Adaptability: 1 – As this process is only to be used for one mission the process does not have the same need for adaptability as the cases that will consider multiple missions. Adaptability is given a weighting greater than zero as some adaptability should be considered when considering an ISM process.
- ISRU Compatibility: 0 – ISRU has not been scoped for this mission, for a short-term mission it would be challenging to gather and utilised resources in space inside the mission lifetime.

The weighted comparison for the short-term case is shown in Table 3-4 below. These weighting has been estimated by the author. The score is the product of the unweighted score and the weighting.

Table 3-4 – Weighted comparison of short-term ISM mission

Process	Weighting	DED	FDM	PVD	Solid Foams
Deployment Time	2.5	7.5	5	2.5	12.5
Ease of Automation	2	4	6	4	4
Adaptability	1	2	3	4	2
Resource Effectiveness	2	6	6	6	6
Reliability	2	6	8	6	4
ISRU compatibility	0	0	0	0	0
Total	-	25.5	28	22.5	28.5

The weightings used for the medium-term case are listed from highest to lowest below:

- Ease of automation: 2.5 – As this system is intended to operate over a longer mission any additional operations that are required to support the process on orbit would require on-going support throughout the mission which incurs a significant cost.
- Reliability: 2.5 – This system is intended to make products for other missions and enhance their capabilities, as such, the reliability of the products made by this system are significant.
- Adaptability: 2 – This system will service other missions so a system that is more adaptable and can change its product to suit the needs of new missions could be advantageous.
- Resource effectiveness: 1.5 – In this case, it is expected that the ISM platform will be resupplied, while resource effectiveness is still important, it would be possible to supply the mission with additional resources to make up for resources that are not used effectively.
- Deployment time: 1 – As this is a longer mission more time can be allotted to deploying products and so the deployment time is less significant than in the short-term case.
- ISRU Compatibility: 0.5 – This mission is intended to be resupplied so it is not dependent on using resources in situ. However, if this system is able to utilise in-situ resources it may reduce the need for resupplies and help make the system more independent.

The weighted comparison for the medium-term case is shown in Table 3-5 below. These weighting has been estimated by the author. The score is the product of the unweighted score and the weighting.

Table 3-5 – Weighted comparison of medium-term ISM mission

Process	Weighting	DED	FDM	PVD	Solid Foams
Deployment Time	1	3	2	1	5
Ease of Automation	2.5	5	7.5	5	5
Adaptability	2	4	6	8	4
Resource Effectiveness	1.5	4.5	4.5	4.5	4.5
Reliability	2.5	7.5	10	7.5	5
ISRU compatibility	0.5	0.5	0	1	0
Total		24.5	30	27	23.5

The weightings used for the long-term case are listed from highest to lowest below:

- Ease of automation: 2 – This system is intended to make a large structure over a long time and so any operator support could become a significant cost and, as such, automation would be very important to such a system.
- Reliability: 2 – The consistency of products made by this large-scale process would be important given the need for automation.
- Adaptability: 2 – Given the scale of this construction it is possible that the production plan may have to update and adapt to complete the build, in this case, adaptability would be an important characteristic.
- ISRU Compatibility: 1.5 – The scale of this construction would mean that a significant amount of mass would have to be transported to orbit from the ground at great cost, a system that was capable of ISRU may not have this cost.
- Resource effectiveness: 1.5 – As it is intended for this mission to be either resupplied or to find supplies in-situ, the need for resource efficiency is similar to that of the medium-term case.
- Deployment time: 1 – While still important for this case the overall deployment time is of less importance than it would be on a shorter-term mission as it may take up less of the overall mission time.

The weighted comparison for the long-term case is shown in Table 3-6 below. These weighting has been estimated by the author. The score is the product of the unweighted score and the weighting.

Table 3-6 – Weighted comparison of long-term ISM mission

Process	Weighting	DED	FDM	PVD	Solid Foams
Deployment Time	1	3	2	1	5
Ease of Automation	2	4	6	4	4
Adaptability	2	4	6	8	4
Resource Effectiveness	1.5	4.5	4.5	4.5	4.5
Reliability	2	6	8	6	4
ISRU compatibility	1.5	1.5	0	3	0
Total		23	26.5	26.5	21.5

As shown in the comparison across the cases, solid foam is more suited to short term missions where the requirement for a rapid deployment of the in-space manufactured products is needed. In these cases, solid foams have key advantages for high volumetric print rates and low energy demand which make it appealing. However, solid foam's poor reliability makes it less advantageous for longer term missions where slower processes that produce higher quality product can be used. The weightings used in this case have been decided by the author based on representative cases. It is possible that the weightings in a more specific example could be different and the specifics of any mission using ISM could change the outcome of this comparison.

Other decisions matrices were considered for this comparison, including the Pugh decision matrix [64]. It was decided that, in this case, the Pugh would not be as effective as decision matrix used due to a number of factors:

- It is difficult to assign a datum concept and evaluate performance against that when all the concepts presented are very early in development.
- The Pugh was considered to be too course a tool as it was only possible to show small increments of improvement or regression (typically being limited to only two increments of improvement or regression).
- A Pugh matrix would not have been able to show that a concept does not meet a criteria altogether (i.e. a process scoring a "0" on a criteria), which was used to show wither or not a process conformed with a non-critical process (as is the case in the example of FDM and Solid Foams for ISRU). In practical terms this would be similar to a product non-conforming to a "should" requirement rather than a "shall" requirement, while this would have an impact on the selection it would not invalidate the use of the product for a task provided it meet the other requirements.
- It was not clear that a Pugh matrix would have provided a more objective tool given that the inputs to the matrix would have been based on same evaluation as is shown above.

4. Solid Foams in Comparable Use Cases

In order to better understand the characteristics of a solid foam material ISM process, when used to construct a large space structure, solid foams and their manufacturing processes were compared with other ISM materials and processes over a range of example cases. The results of this comparison were first reported on by Hastie, Bailet and McInnes in "On-Orbit Manufacturing of Large Space Structures Using Solid Foams" presented at the 72nd International Astronautical Congress [10]. This chapter will discuss the motivation behind this research, the methods used to gather the results and discuss the limitations of the research.

4.1 Motivation

The motivation for this study came from an interest in exploring systems that could take advantage of the unique qualities of solid foams that have been discussed in both the trade-off and the literature review chapters. The main qualities that the study explores in more depth are:

- Short deployment times
- High resource effectiveness
- Adaptability

As discussed in the trade off chapter, solid foams have a higher volumetric printing rate that other AM processes. In order to understand the impact of this high volumetric print rate the construction time of products made using each of these methods was compared. To provide a practical example, each of the products compared had to have the same functionality in its given use case.

As discussed in earlier chapters, the low density of solid foams means that solid foams have a high packing ratio (the ratio of input material volume to output product volume). This high packing ratio shows that solid foams have a high resource effectiveness when only the volume of the product is considered. The effects of this high packing ratio are shown Figure 4-1 below, in which a 3D model shows how the volume of a cube of foam with varying relative densities, but the same solid mass, changes in volume when the cells are dispersed evenly. As discussed in the literature review, chapter 2 section 3, the mechanical material properties of a foam are also varied with foam density. The Gibson-Ashby equations for foam mechanical properties [30] suggest that the elastic modulus, bulk modulus and compressive strength of a solid foam all vary inversely with the foam's relative density and packing ratio. This suggests that there may be an interesting trade-off between that packing ratio of solid foams and the weaker material properties when compared to other AM. To explore this further this study used a comparison between products made with various manufacturing processes, but with the same functionality, and explored if it would be possible for a solid foam structure to provide the same functionality with less resources than the other AM process considered.

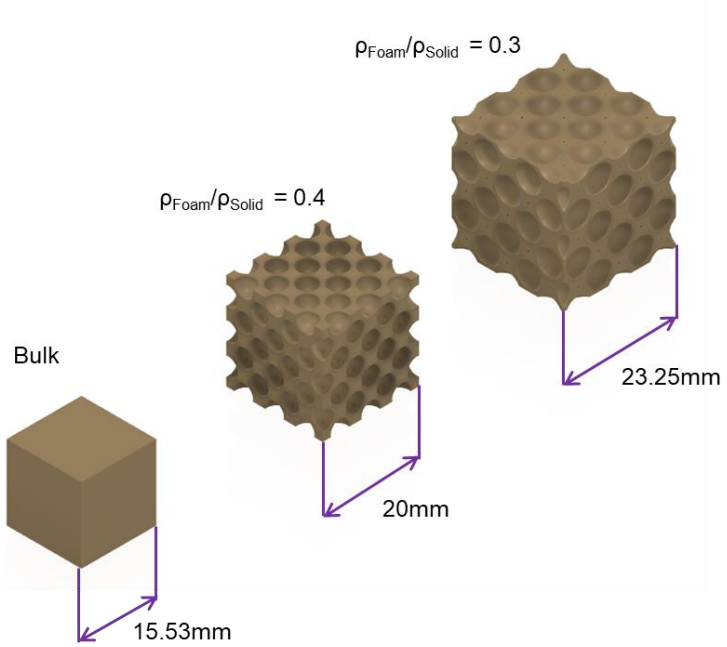

Figure 4-1 – 3D model of foam cubes with varying relative densities, all models have the same solid mass presented in Hastie et al [10]

In chapter 3 section 4, it was reported that the solid foam production process requires less power than other comparable manufacturing processes. As with the material resources, this provides an interesting comparison, as while the solid foams require less energy to produce a product of the same mass, when compared with other ISM processes, the material produced may have less optimal structural and thermal properties. Once again, a functional equivalent product comparison was conducted to explore the trade-off between solid foam and other ISM processes.

Chapter 2 section 3 identifies multiple use cases for solid foams, notably thermal insulation and structural support. The ability to make use of solid foams for more than one application makes the process more adaptable. To investigate this adaptability, both thermal and structural use cases were explored to better understand adaptability of the process and consider the trade-offs that an adaptable process would have.

4.2 Scope of Case Studies

The chapter will now consider two cases, one where the ISM process is used to make a structural support and one where the ISM process is used to make an insulating layer. In each case an ISM product was constructed using a range of hypothetical ISM processes. The products used for each comparison all provided the same function.

In the structural case, the product was a simply supported cantilever beam supporting a point load at a set distance. Each of the beams compared had the same cross-sectional shape (a simple square), the same arm length and the same load. The length of the sides of the square cross section were adjusted so that the beam provided the same resistance to the bending load, as shown by each of the beams having the same factor of safety, with respect to material strength.

In the thermal case, a solid foam sunshade was compared with an MLI system with the same thermal gradients between the sun facing and platform sides of the shade. The MLI shade was made of two thin film layers made of aluminium and produced using PVD and a frame, to hold tension across the film and separate the film layers, made of PEEK. This frame would be constructed using an FDM process. Both shades where square in shape, had the same area and provided the same thermal gradient when the shade is sun pointing and the payload is at room temperature. The design of the MLI systems was proposed and the thickness of the foam system was selected to match the temperature gradient of the MLI sunshade.

In both cases the design of the product was simple to make for a more direct comparison across approaches.

4.3 Methodology

4.3.1 Cantilever Beam

As discussed in section 2 of this chapter, the beam length, cross-sectional shape, load and factor of safety remained consistent across each example. A diagram of the beam is shown in Figure 4-2 below:

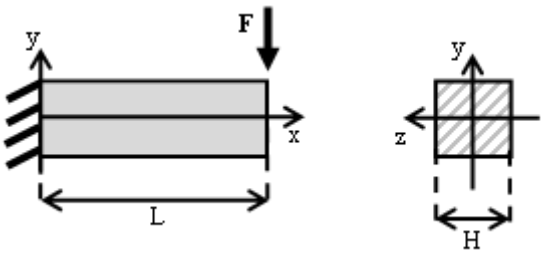

Figure 4-2 – Diagram of cantilever beam

Here, F is the applied force, which is 1 N in this case, L is the beam length, which is 1 m in this case and H is the beam thickness, which varies depending on the material used. The Factor of Safety (FoS) with respect to yield strength remains constant at 2 across the material choices. The factor of safety is calculated using Eq. 4-1 below.

$$FoS = \frac{\sigma_{Max}}{\sigma_{Yield}} \qquad 4\text{-}1$$

Here, σ_{Max} is the maximum tensile stress experienced by the beam and σ_{Yield} is the tensile yield strength of the beam material. The maximum tensile stress was calculated using the Euler–Bernoulli beam theory, with the assumption that the cross section of the beam remains normal to the length of the beam at any point along the beam, as discussed by Megson [65, p. 9]. The maximum stress was found using Eq.4-2 below

$$\sigma_{Max} = \frac{Mo_{Max}\, y_{Max}}{I} \quad 4\text{-}2$$

Here, Mo_{Max} is the maximum bending moment experienced on the beam, y_{Max} is the distance from the neutral bending axis to the outer surface of the beam and I is the second moment of area. The maximum bending load occurs at the base of the beam where it meets its support and is equal to the product of the load and the beam length. The bending occurs symmetrically around the centre of the beam as the beam is evenly supported at its base, as such, the maximum distance from the bending axis is equal to half the beam's thickness. The second moment of area for the section has been calculated using Eq. 4-3 which has been derived from Megson [66].

$$I = \frac{H^4}{12} \quad 4\text{-}3$$

Using these relationships the thickness of the beam was calculated using Eq. 4-4 below.

$$H = \sqrt[3]{\frac{6\, F\, L\, FoS}{\sigma_{Yield}}} \quad 4\text{-}4$$

The print time and energy usage were calculated using the process rates discussed in chapter 3 section 1.

4.3.2 Sunshade

As discussed in section 2 of this chapter, the sunshade must have the same thermal gradient when the payload is held at room temperature. While both systems provide the same thermal gradient, this is achieved via different designs. The MLI is made up of 2 sheets of thin aluminium and the foam sunshade is a consistent coating across the same surface area. Both systems are square in shape and have edges of 150 m. Macro scale sunshades of the scale considered here could be used to protect large space telescopes from high thermal loads or prevent cryogenic fuel tank boil off in a similar manner to the insulators considered by Xiaodai et al [59]. One face of the system will face the sun and the other will face a nominal payload.

The MLI case considered was constructed of two aluminium thin film layers each of which is 25 μm thick. The layers are tensioned using a cross shaped tensioning frame, made up to 4 tube shaped trusses constructed from PEEK. It is similar in shape to the solar sail investigated by Sleight and Muheim [67]. A schematic of this system is shown in Figure 4-3 below.

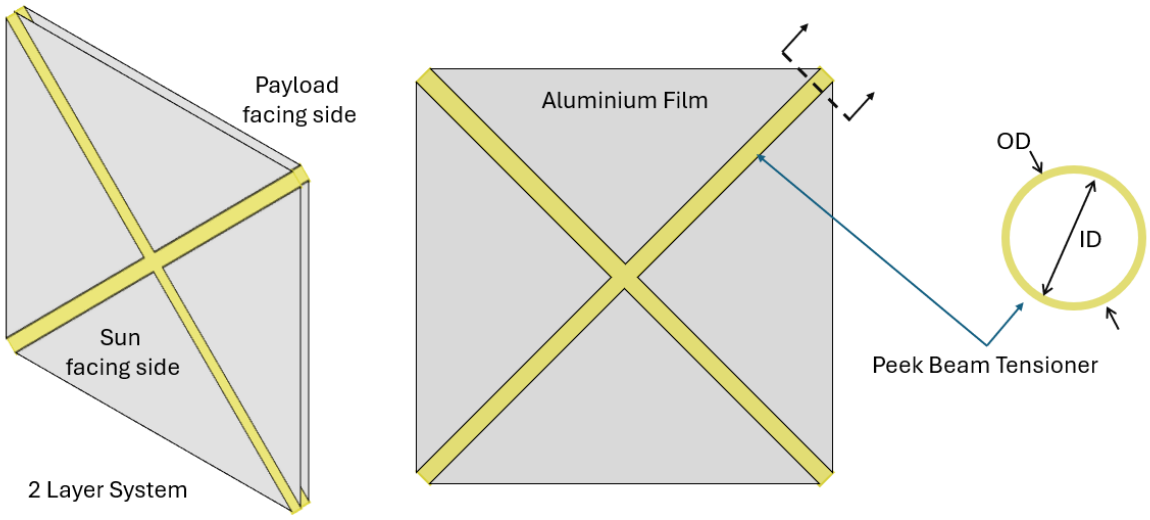

Figure 4-3 – Multilayer system design diagram (not to scale)

Here OD is the outer diameter of the tube which was 100 mm and ID is the internal diameter of the tube which was 98mm. It was assumed there was little to no heat exchange across the frame and that each film had a perfect view factor of the next one. To calculate the temperature gradient across the system the heat exchange between the inner and outer layers of each of the films was considered when the heat flux was set to the mean solar heat flux. Within the same film the temperature gradient was calculated using conduction and between the films the temperature gradient was calculated using radiative heat exchange. The system was divided into five nodes:

1. The payload
2. The surface of the layer closest to the payload that is facing the payload
3. The surface of the layer closest to the payload that is facing the sun
4. The surface of the layer closest to the sun that is facing the payload
5. The surface of the layer closest to the sun that is facing the sun

A diagram of this nodal system is shown in Figure 4-4 below.

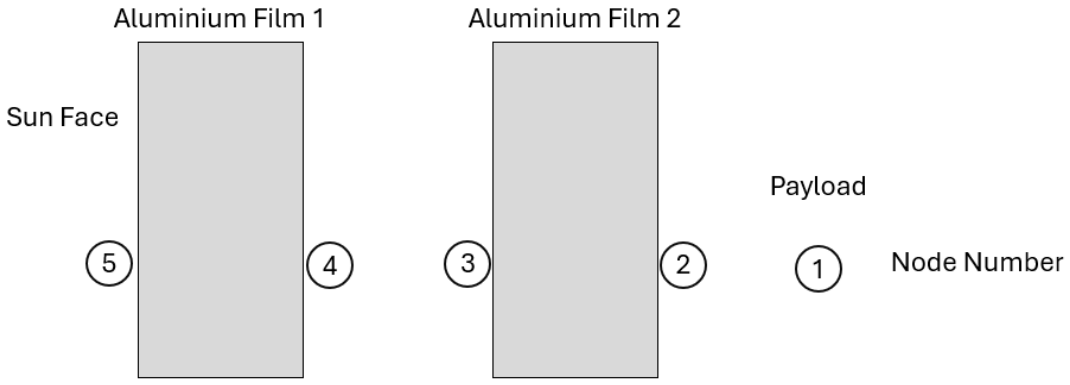

Figure 4-4 – Multilayer system thermal nodes

The Stefan-Boltzmann law can be used to calculate the radiative heat exchange between two planar grey bodies, as described by Balaji et al [68] using the radiosity-irradiation method, as shown in Eq. 4-5 below.

$$q = \frac{SBC\left(T_a^4 - T_b^4\right)}{\frac{1}{\varepsilon_a} + \frac{1}{\varepsilon_a} - 1} \tag{4-5}$$

Here q is the heat exchanged per unit area, T is the temperature for either body a or b, ε is the emissivity of the surface and SBC is the Stefan-Boltzmann constant. The heat exchange through the thin film can be calculated using conductive heat exchange, as described by Balaji et al [69] , as shown in Eq. 4-6 below.

$$q = -k\frac{\partial T}{\partial x}$$
$$q = -k\frac{\Delta T}{w} = -k\frac{T_a - T_b}{w} \tag{4-6}$$

Here k is the thermal conductivity of the material, T_a and T_b are the temperatures of surfaces a and b respectfully on either side of the material the difference and w is the thickness of the material.

Using equations 4-5 and 4-6 above the temperatures of each node in the system can be found based on the temperature of node 1.

$$T_2 = \sqrt[4]{\frac{q\left(\frac{1}{\varepsilon_2} + \frac{1}{\varepsilon_1} - 1\right)}{SBE} + T_1^4} \tag{4-7}$$

$$T_3 = \frac{qw_{Film}}{k} + T_2 = \frac{qw_{Film}}{k} + \sqrt[4]{\frac{q\left(\frac{1}{\varepsilon_2} + \frac{1}{\varepsilon_1} - 1\right)}{SBE} + T_1^4} \tag{4-8}$$

$$T_4 = \sqrt[4]{\frac{q\left(\frac{1}{\varepsilon_4} + \frac{1}{\varepsilon_3} - 1\right)}{SBE} + T_3^4} = \sqrt[4]{\frac{q\left(\frac{1}{\varepsilon_4} + \frac{1}{\varepsilon_3} - 1\right)}{SBE} + \left(\frac{qw_{Film}}{k} + \sqrt[4]{\frac{q\left(\frac{1}{\varepsilon_2} + \frac{1}{\varepsilon_1} - 1\right)}{SBE} + T_1^4}\right)^4} \tag{4-9}$$

$$T_5 = \frac{qw_{Film}}{k} + T_4 = \frac{qw_{Film}}{k} + \sqrt[4]{\frac{q\left(\frac{1}{\varepsilon_4} + \frac{1}{\varepsilon_3} - 1\right)}{SBE} + \left(\frac{qw_{Film}}{k} + \sqrt[4]{\frac{q\left(\frac{1}{\varepsilon_2} + \frac{1}{\varepsilon_1} - 1\right)}{SBE} + T_1^4}\right)^4} \quad 4\text{-}10$$

The temperature over the entire thermal gradient can then be found using the following equation.

$$\Delta T = T_5 - T_1 \quad 4\text{-}11$$

The temperature gradient, ΔT, found in Eq. 4-11 can also be used in Eq. 4-6 to calculate the thickness of a foam, w, that would be required to achieve the same the same thermal gradient as the MLI system.

The print time was calculated by taking the sum of the time taken to print each element of the system. An element's print time was calculated as the time it would take to print the volume of that element using a uniform volumetric print rate for that material. The volumetric print rates for each material used are discussed further in section 4.4.

The MLI system consisted of 3 elements – 2 films and a tensioner frame. The volumes of the films were calculated as the product of the overall sunshade area – 150 m x 150 m – and the thickness of the film – 25 μm thick – which is discussed earlier in this section. The volume of the tensioning frame was calculated as the product of the cross-sectional area of the frame (as set out in Figure 4-3) and the length of the frame's arms. The films and frames were printed using a PVD and FDM printing process, respectively, the volumetric print rate for each of these processes is discussed further in section 4.4.

The volume of the foam system was calculated as the product of the overall sunshade area – 150 m x 150 m – and the foam material thickness required to meet the temperature gradient calculated in Eq. 4-11.

The energy required to construct each system was found as the product of the total print time and the power required to use the ISM process.

It was assumed in the study that the sun facing side of the shade received full solar flux. However, Gibsons's "Spacecraft thermal control handbook" [56] suggest that the heat flux into a surface can be calculated as the product of the incoming heat and the surface absorptivity. If this modification is applied, then it would result in a reduction in the heat flux into the system as surface absorptivity must be less than 1.

4.4 Case Parameters

4.4.1 Cantilever Beam

As discussed earlier, the length of the beam and the load that it is supporting is 1 m and 1 N respectfully so the maximum bending moment is 1 Nm. The tensile yield strength and density for each of the materials used in the study is shown in Table 4-1 below along with its source. Where possible the material strength and density values cited have come from sources, in which the material studied used the same forming processes as the material considered in this comparison study. For example, the strength of PEEK used below is based on the results of PEEK samples produced using FDM and not a PEEK sample that has been injection moulded or machined.

Table 4-1 – Cantilever case material properties

Process & Material	**Tensile Yield Strength, σ_{Yeild} (MPa)**	**Density, ρ (kg/m^3)**	**Sources**
Sold Foam, PUF	1.99	160	PCF10 reported by Horak et al [70]
FDM, PEEK	87.34	1300	Strength – PEEK 450G™ reported by Li and Lou [51] Density – Vitex™ PEEK 450G™ datasheet [71]
DED, 316 Stainless Steel	558	7990	Reported by Zhang et al [53]

As well as the material properties, this study also considered the process parameters of print rate and power consumption to understand the total construction time and the total energy consumption needed. There are fewer direct sources of information on this available when compared with the material properties. The process parameters used in this study are shown in Table 4-2 below, the sources of information and justification is shown for each parameter.

Table 4-2 – Cantilever case process properties

Process	Volumetric Print Rate, $\dot{V}$ (mm^3/s)	Mass Print Rate, $\dot{M}$ (g/s)	Power consumption, P (W)	Sources
Sold Foam	2178	0.054	41.73	Print rate – As reported by Barnett and Gosselin [50] Power – See note [1]
FDM	3.770	4.901×10^{-3}	139	Print rate – Based on the reporting of Li and Lou [51] Power – reported by Hassan et al [72] for a full in fill using the Apium P220 FFF
DED	1.69	1.4×10^{-2}	1000	Based on the layer hight and print rate reported by Zhang et al [53]

[1] There is no reporting of the power consumption for the foam dispersal system used by Barnett and Gosselin [50], it is possible that a pressurised container was used instead of a continuous pump. To provide an example of the power that would be required for a PU foam dispersion, a pump was selected that can provide the same flow rate as the peak flow rate reported by Barnett and Gosselin. The power consumption was then found by assuming that the power scaled linearly with the flow rate and considering the volumetric flow rate above. The example pump used was a Alchatek™ IMPACT 440 [73], which is capable of a peek flow rate of approximately 34068.7 mm^3/s (0.54 gallons per minute) and a peek power consumption of 652.75 W (7/8 electrical horsepower). If the power consumption linearly scales with the flow rate, then for a mean flow rate of 2178 mm^3/s the power consumed would be 41.73 W.

4.4.2 Sunshade

Many of the same processes and materials are used in the sunshade and cantilever beam cases, this section shows the new or modified parameters.

There are thermal properties that were used in the sunshade example that are not considered in the cantilever beam. Thermal conductivity for both the foam and the aluminium are considered. The foam used is polyurethane and the value used for thermal conductivity is 0.025 W/mK, which is reported by Gibson and Ashby [30] and is similar to values presented by Zhang et al [74] and Tibério Cardoso et al [75]. The metallic film used in the MLI system is made of aluminium, Zhang

and Li [76] report a thermal conductivity for pure aluminium of 237 W/mK and aluminium alloys ranging from 92 W/mK to 152 W/mK. Given that this is aluminium made in the process described by Lippman [13] , in which some of the spacecraft structure is reused after launch, it would be consistent to base the thermal conductivity on an aluminium alloy that is used for this purpose. For this reason, the thermal properties of aluminium 6061, which is used in spacecraft structures, was used. Gilmore [56] reports aluminium 6061 as having a thermal conductivity of 180 W/mK.

The thermal optical properties for the aluminium sheet must be considered in the multilayer thermal insulation case. An emissivity and absorptivity of 0.02 and 0.08 is reported by Gilmore [56] for vapour deposited aluminium. Aluminium 6061 has a density of 2700 kg/m^3 as reported by Adediran et al [77]

The process parameters for the PVD process have been derived from the study reported by Lippman [13], in which a print rate of 0.2 kg per hour ($5.6x10^{-2}$ g/s) is achieved with a system that consumes 2640 W of power. The sheet thickness was 2.5 µm. The density of aluminium used was 2700 kg/m^3.

4.5 Results

4.5.1 Cantilever Beam

The beam thickness calculated using Eq.4-4 and the parameters detailed section 4.4, are shown in Figure 4-5 and Table 4-3 below.

Table 4-3 – Thickness of square section required to the support load for the cantilever case

Material	Foam	PEEK	Stainless Steel
Beam Thickness, H (mm)	18.20	5.16	2.78

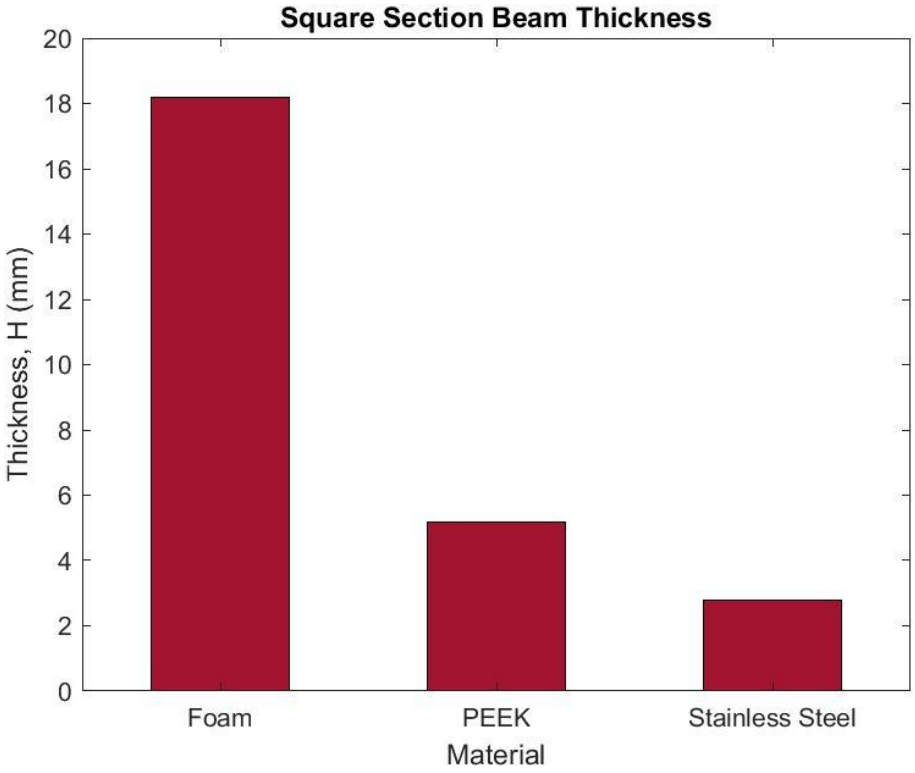

Figure 4-5 – Thickness of square section required to support the load for the cantilever case

The beam mass, calculated using cross sectional area and length to find the volume, and the density detailed in section 4 of this chapter, are shown in Figure 4-6 and Table 4-4 below.

Table 4-4 – Mass of beam required to support the load for the cantilever case

Material	**Foam**	**PEEK**	**Stainless Steel**
Beam Mass, M (g)	53.01	34.62	61.79

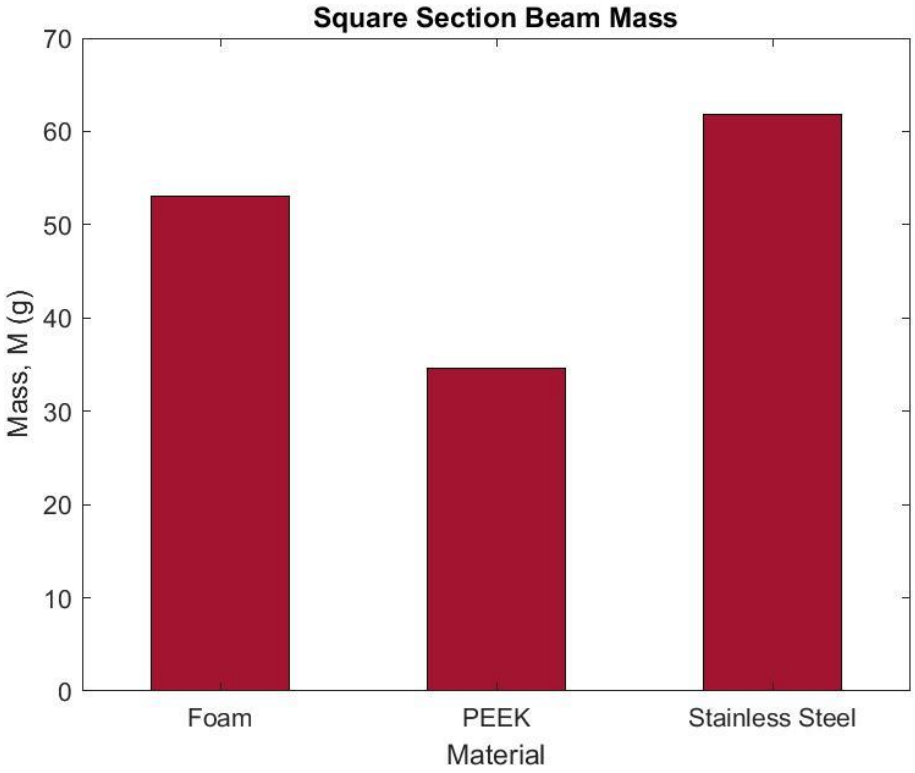

Figure 4-6 – Mass of beam required to support the load for the cantilever case

The time taken to print the beam, calculated using the cross-sectional area and length to find the volume and the volumetric print rates set out in section 4 of this chapter, are shown in Figure 4-7 and Table 4-5 below.

Table 4-5 – Time taken to produce beam required to support the load for the cantilever case

Material	**Foam**	**PEEK**	**Stainless Steel**
Beam Production Time, t (s)	152	7.06×10^3	4.56×10^3

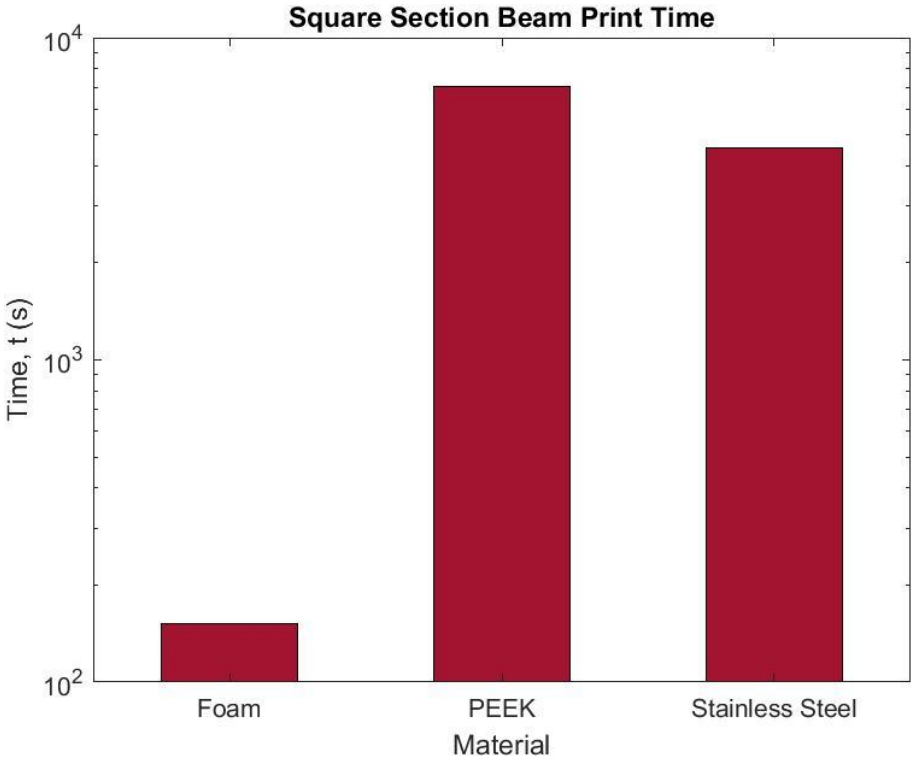

Figure 4-7 – Time taken to produce beam required to support the load for the cantilever case

The energy consumed to create the beam, calculated as the product of the beam print time and the average power consumption detailed in section 4 of this chapter, are shown in Figure 4-8 and Table 4-6 below.

Table 4-6 – Energy consumed to produce beam required to support the load for the cantilever case

Material	Foam	PEEK	Stainless Steel
Beam Production Energy, E (J)	6.35×10^3	9.82×10^5	4.57×10^6

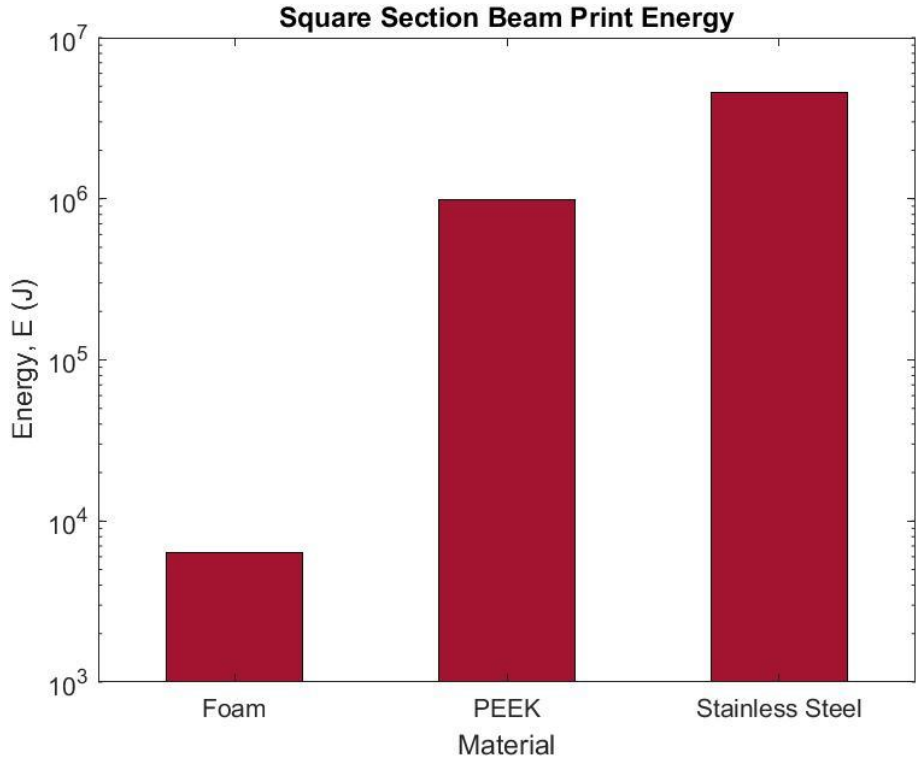

Figure 4-8 – Energy consumed to produce beam required to support the load for the cantilever case

4.5.2 Sunshade

Using the parameters set out in section 4 of this chapter and Eq. 4-11 it was found that the multilayer system can provide a temperature gradient of 1188 °C between the sun facing side of the system and the payload when the heat flux through the system is equal to the solar flux. To meet this temperature gradient, when solar heat flux is applied, the foam layer system must have a thickness of 21.6 mm. A gradient of 1188 °C represents what this multilayer system could theoretically hold if the heat flux is equal to the maximum solar flux. However, in practice, it is possible that this heat flux would not be realised, as some of the solar flux would not be absorbed by the surface of the sun facing side of the system and more heat being reject to space, as the temperature of the sun facing film increased. While this gradient is unlikely, it shows what the multilayer system is capable of and provides a maximum gradient that a foam layer can be compared with in term of construction time and energy.

The total mass for both the multilayer system and the foam layer system using are shown in Figure 4-9 and Table 4-7 below. These masses have been calculated as product of the system volume, found using the process outlined in section 3 of this chapter, and the material density detailed in section 4 of this chapter.

Table 4-7 – Mass required for each system in sunshade case

System	Foam	Multi-layer (Thin film/ Frame)
Sunshade Mass, M (kg)	7.79×10^4	304/ 172

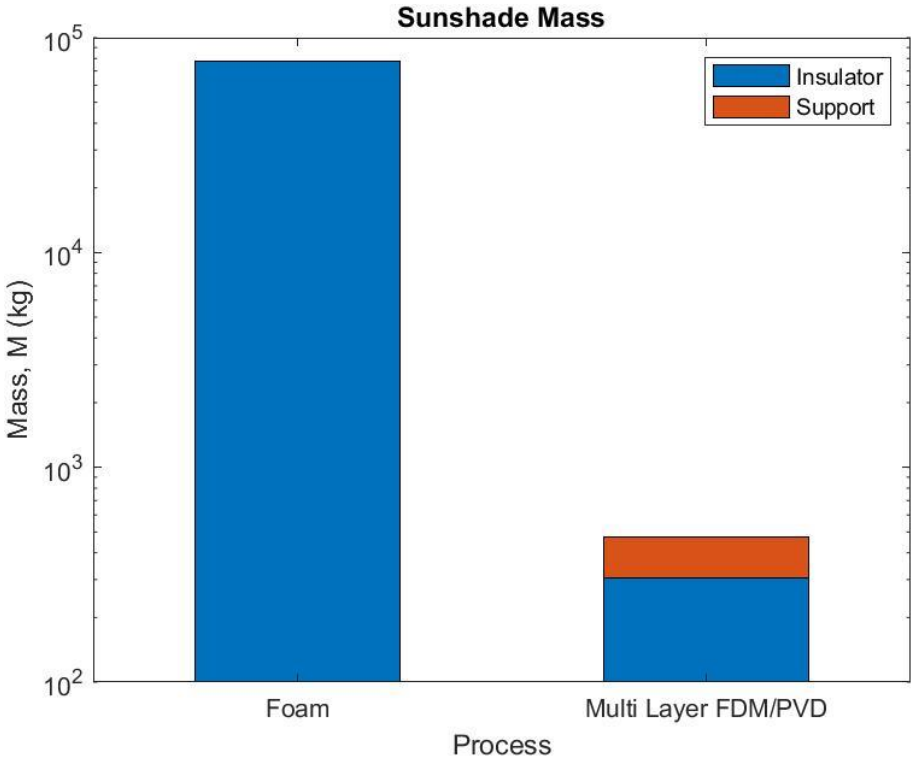

Figure 4-9 – Mass required for each system in sunshade case. For the foam system the insulator is the foam, for the multilayer system the insulator is the aluminium film and the support is the PEEK frame

The total print times for both systems were calculated, using the process outlined in section 3 of this chapter, are shown in Figure 4-10 and Table 4-8 below.

Table 4-8 – Time taken to produce each system in sunshade case, using updated process parameters

System	Foam	Multi-layer (Thin film/ Frame)
Sunshade Print Time, t (s)	2.23×10^8	5.47×10^6/ 8.18×10^7

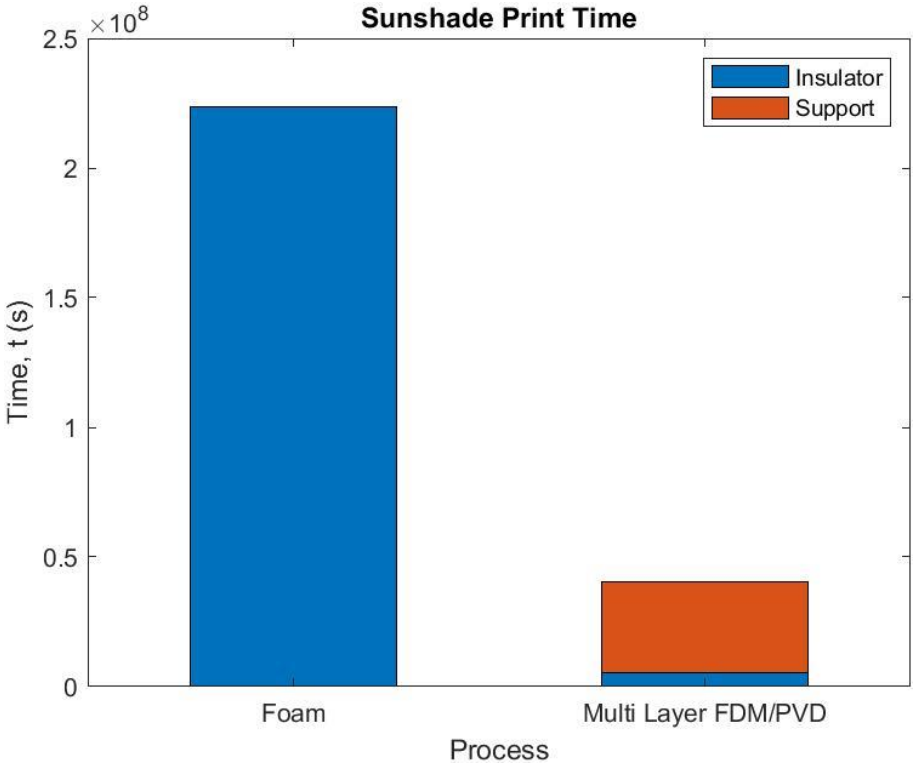

Figure 4-10 – Time taken to produce each system in sunshade case. For the foam system the insulator is the foam, for the multilayer system the insulator is the aluminium film and the support is the PEEK frame.

The total print energy for both systems was calculated, using the product of the total print time shown above and the average power detailed in section 4 of this chapter, are shown in Figure 4-11 and Table 4-9 below.

Table 4-9 – Energy consumed to produce each system in sunshade case

System	**Foam**	**Multi-layer (Thin film/ Frame)**
Sunshade Print Energy, E (J)	9.32×10^9	1.44×10^{10}/ 8.18×10^9

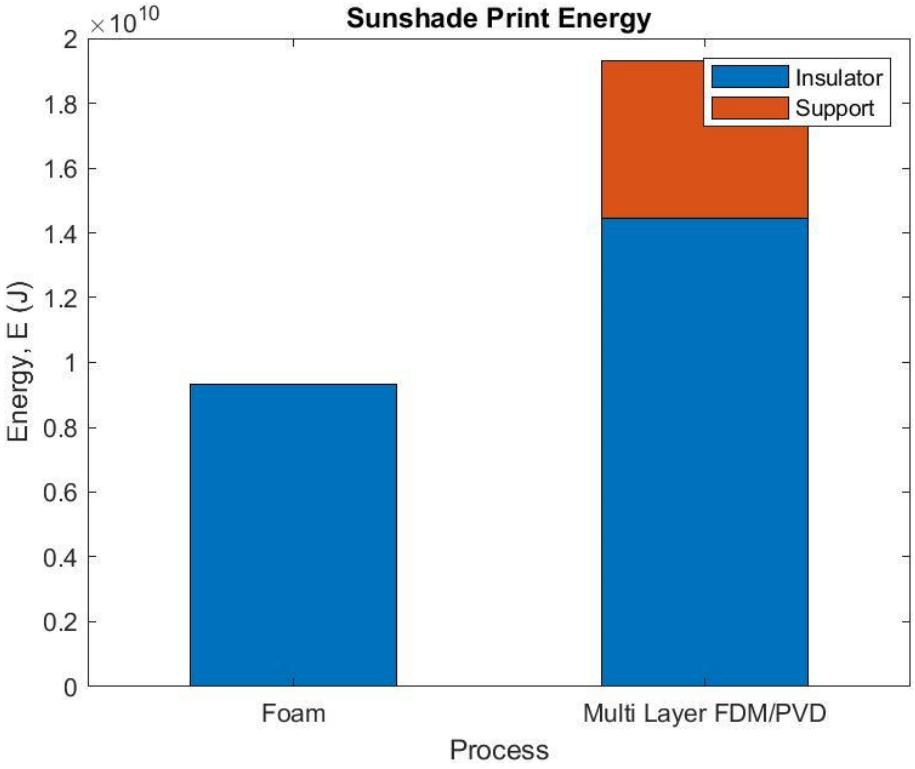

Figure 4-11 – Energy consumed to produce each system in sunshade case. For the foam system the insulator is the foam, for the multilayer system the insulator is the aluminium Sheet and the support is the PEEK frame.

4.6 Discussion

When comparing simply supported cantilever beams it was found that the foam material required the thickest section followed by the PEEK beam, with the steel beam requiring the smallest section as is shown in Figure 4-5. This is not a surprising result given that Eq. 4-4 that the thickness of the beam is inversely proportional to the material strength. When comparing the cantilever beam's mass, it was found that, while foam required the thickest beam section, its relatively low density meant that this beam's mass was less than that of the stainless steel beam, while still greater than that of the PEEK beam, as shown in Figure 4-6.

When comparing the deployment time, the foam printing process takes the shortest time, with the stainless-steel process the second shortest and the FDM process taking the longest, as shown in Figure 4-7. The solid foam deployment time is significantly shorter than the next shortest deployment time (stainless steel DED) with a difference of almost two orders of magnitude between the foam printing process and the DED process.

When comparing the energy required to produce the beam, it is clear that the foam printing process takes significantly less energy than the FDM or stainless-steel DED processes, with the DED process being the most energy intensive. This solid foam process requires more than two orders of magnitude less energy than the FDM process, as shown in Figure 4-8.

When comparing the sunshade case solutions, it can be seen that the foam solution requires more mass than the multi-layer solution would, as shown in Figure 4-9. The deployment time of the foam is around four times greater than that of the multi-layer system, as shown in Figure 4-10. The foam solution was shown to require less energy to construct than the multi-layer solution requiring around half as much energy, as shown in Figure 4-11.

In both cases, the foam product provides a similar function to the comparable products by providing either a thicker, in the case of the beam, or more massive, in the case of the shade, product. This is not surprising, given that the material properties of the foam for both mechanical strength and thermal transportation are less favourable than the material or systems that it has been compared with. Notably, in both cases, it can be seen that the foam printing process requires less energy than any of the other process that it is compared with, in the case of the cantilever beam this is quite significant, with the foam requiring two orders of magnitude less energy to construct the beam than the comparable processes. Similarly, foam shows an advantage when it comes to deployment time in the cantilever beam case and a similar print time in the sunshade case.

A simple comparison of the process and material parameters of a foam printing process could predict that the foam printed product would be larger and the printing process would have a higher print volume rate. However, his study shows that, when the products created have a comparable function, a foam printing process may be able to produce this product in a shorter time and use less energy to do so. This suggests that foam may be a useful solution for products manufactured in space when the spacecraft has low power generation capabilities, or a short mission life as was suggested in the trade-off chapter.

4.7 Limits of the Study

The outcomes of this study have been limited by the assumption and simplifications that where applied. A notable example is the limitation on the complexity of the cases studied. While this is somewhat deliberate, to remove case specific variability for the study, it is unlikely that such simple use cases will be applied in practice. For example, the loading described in the cantilever case is unlikely to be so simply loaded, with a more likely example involving a more variable load in both scale and direction, as well as more specifics on the application of any such load. It is likely that more complex examples would increase the additional mass required for the foam beam compared to the other materials, but it is not clear at what point a more complex foam beam would require more energy or time to produce than either a PEEK or stainless-steel beam. A more complex case could be used to study this in more depth, and understand at what stage the additional volume of foam required would result in a longer foam print time or a foam print that requires more energy than the PEEK or steel equivalents.

In the sunshade case, no maximum temperature was considered. Given that the temperature gradients reported were greater than 500 K, changes in the material property and state could be expected. This would indicate that both systems would be invalid in the case as it is currently presented. A more detailed case, which considers the heat lost to the environment, as well as the heat absorbed due to solar radiation, could be a more suitable comparison. Such a case could

explore the thermal optical properties – such as the solar absorptivity and IR emissivity – of a foam system and potentially how these thermal optical properties could be adjusted with doping.

In the cantilever case, only the strength of the beam was considered as a criteria, the displacement of the beam was not considered. The displacement of the beam may be an important consideration for such a study, as the assumption behind the Euler–Bernoulli beam theory assumes a small displacement relative to the beam size. Additionally, the displacement of the beam could have an impact on component alignment or the loading on other structural parts. Further study could be conducted that looked at comparing the beam functionality with respect to displacement as well as strength.

In both cases the material and process properties are derived from the literature. A more practical example could be explored where products are built using a variety of proposed ISM processes, and then tested. This would provide a more practical comparison than the one presented but would limit the comparison to processes as applied in that test. Ideally, these practical examples would be produced in conditions similar to those found on orbit, i.e. in vacuum and under micro gravity.

5. Solid Foams for Aerocapture Around Mars

To further explore the characteristics of a solid foam material ISM process for the construction of large structures, a specific use case was considered. To this end research was conducted into the use of solid foams as the building material for an aerodynamic decelerator designed to capture a platform traveling on a heliocentric trajectory into orbit about Mars. The results of this research were first reported by Hastie, Bailet, White and McInnes in "The Use of In-Space Manufactured Solid Foams for Aerocapture" at the 18th International Planetary Probe Workshop [11]. This chapter will discuss the motivation behind this research, the methods used to gather the results and discuss the limitations of the research.

5.1 Motivation for the Case Study

As was discussed in chapter 4, generalised and abstracted use cases can be used to trade off the benefits of various ISM processes and explore the cases, in which a foam printing process, and its products, could be advantageous. However, a more specific use case could be used to provide a deeper understanding of the applied design parameters required for any such foam printing process and its products. One specific use case, for large-scale space structures, is the use of large aeroshells for aerocapture manoeuvres. The advantage of a large aeroshell is that the larger surface area of the aeroshell the lower the ballistic coefficient and higher the drag force, and so a higher deceleration will be experienced by the spacecraft, while it traverses a planetary atmosphere. Hence, the larger the spacecraft's aeroshell the shorter the time needed to reduce its orbital velocity from a heliocentric hyperbolic trajectory to the desired captured elliptic trajectory around the chosen planet. The larger the aeroshell of the spacecraft, then the shorter the atmospheric traverse, and the higher the pericentre required. Trajectories that have a higher periapsis pass through a less dense part of the atmosphere and so produce less heat due to friction. A spacecraft that has a larger aeroshell will therefore experience a lower heat flux. This relationship between the aeroshell size and the heat flux on the system is discussed by Dwyer Cianciolo et al [78] , in which the mass of a large aeroshell is compared with the additional mass of rigid Thermal Protect Systems (TPS) required for a small aeroshell that experiences a high heat flux. The larger the aeroshell and shorter the deceleration time the higher the impulse on the aeroshell and so a larger aeroshell will experience a higher overall mechanical load, when compared with a smaller aeroshell. For the overall mass of a large aeroshell to be less than that of a small aeroshell, while it supports a higher mechanical load, the material used to construct the larger aeroshell must have a higher specific strength than the material that is used to make the smaller aeroshell. As discussed in the chapter 2, solid foams have a high specific strength and the possibility of adapting solid foams for an ISM process means that they could be used to produce a largescale aeroshell.

Mars was selected for the aeroshell capture manoeuvre given the number of missions that have been planned to be captured into a Martian orbit in the near future. While this case specifically

considered a mission around Mars, the same principle could be considered for a capture around any planet with an atmosphere.

5.2 Methodology

A large foam aeroshell design was considered in this case study and the design developed further. The refined foam aeroshell's performance was compared with other aerocapture methods that have been proposed or applied, including providing the change in velocity via chemical propulsion. The development of this aeroshell study had three stages:

1. Initial design concept, in which the initial design was proposed
2. Parameterised development, in which the properties of the foam were varied to affect the required trajectory and the refined aeroshell parameters where established
3. Detailed condition study, this step was carried out by Dr Craig White [10] and used a direct simulation Monte Carlo (DSMC) solver which was used to understand the thermal requirements needed for the aeroshell material. This work was based on the solver described by White et al [79].

Initial Concept

The initial design concept was based on an aeroshell that could be printed during the mission's transit to Mars. When in its full aerocapture configuration after transferring to a hyperbolic orbit at Mars, the spacecraft will consist of a cylindrical payload with a 3 m radius and weighing 10 tonnes' Surrounding this payload is a payload thermal protection layer made of foam with a thickness of 0.5 m. Extending from the payload hub, on the side of the payload opposite the direction of travel, is the aeroshell, which has a root thickness h of 1 m and tapers to a point at a radial distance of a. A diagram of the spacecraft is shown in Figure 5-1 and Figure 5-2 below. The radius of the aeroshell is defined in the parameterised development stage.

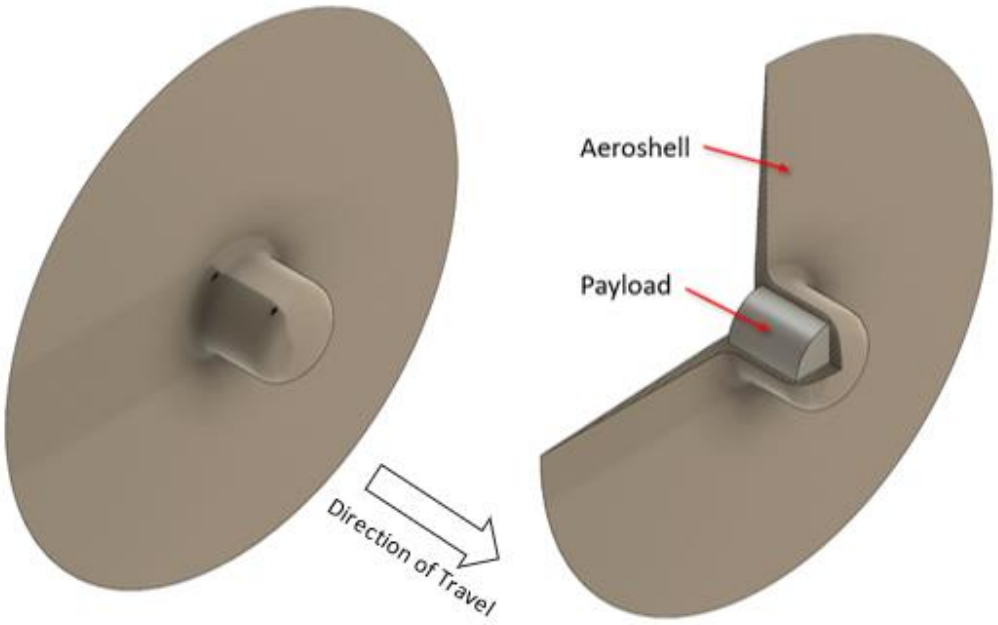

Figure 5-1 – Conceptual design of solid foam aeroshell

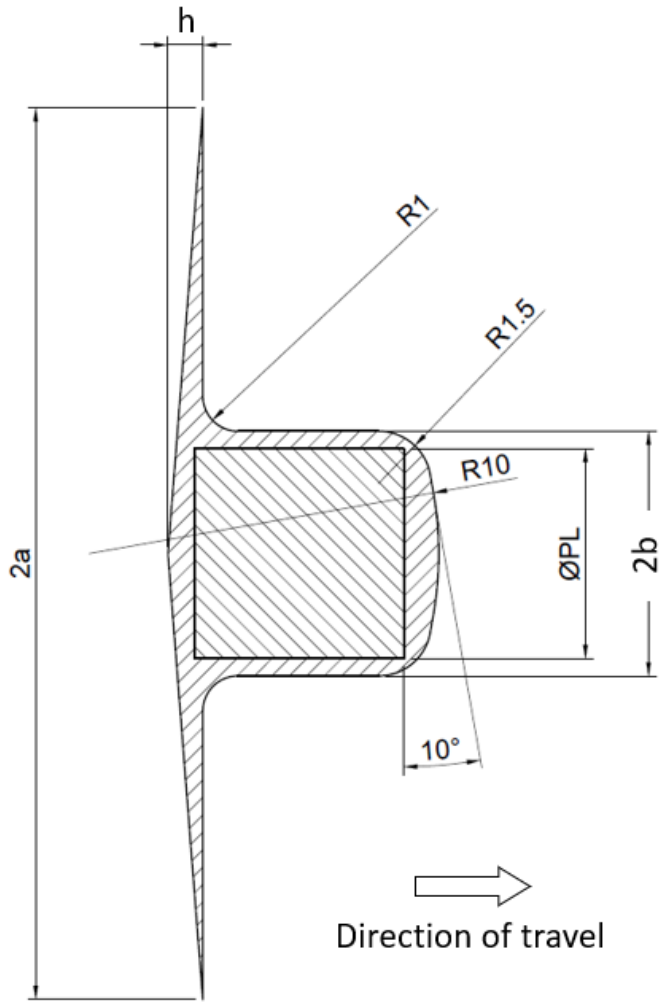

Figure 5-2 – Parameterized diagram of the solid foam aeroshell concept

Here the R1, R1.5 and R10 radii of 1 m, 1.5 m and 10 m, respectively, are constant throughout the parameter study, b is the radius of the payload and its 0.5 m thick TPS (that is a radius of 2 m in total) and ØPL is the diameter of the payload which is 3 m.

Parameterised Development

At this stage a trajectory model, developed by Bailet et al [80], was used to calculate the range of periapsis and trajectories required to capture an interplanetary object in a Martian orbit, with a given ballistic coefficient and set mission mass. The input parameters into the trajectory model where, an initial altitude, an initial flight path angle (γ), the initial speed, the spacecraft mass, its cross-sectional area and it coefficients of drag (C_d) and lift (C_l). Using the initial location and velocity parameters as a starting step, the trajectory model provides the location of the spacecraft after a set timestep, as well as the updated velocity and flight path angle based on the forces acting on the spacecraft. The model then provides the full trajectory of the spacecraft over series of timesteps. The trajectory model considered 3 forces on the spacecraft – the force due to gravity, the drag force and the lift force, again using the model of Bailet et al [80]. This trajectory model was used to plot the trajectories for a range of aeroshell cross-sectional areas and initial flight path angles. The trajectory model terminated when the model run exceeded its allotted time, or the spacecraft altitude fell to zero – indicating that the spacecraft crashed onto the surface. The final timestep velocities, flight path angle and altitude of the spacecraft that do not crash into the surface are logged.

For the logged spacecraft (that is the ones that did not crash) to be considered successful aerocapture its apoapsis must fall with in an upper and lower altitude limit, these limits are discussed in section 3 of this chapter. Two methods were used to determine the apoapsis:

- During the simulation – Bases on the change in altitude of the spacecraft
- After the simulation – Based on the final velocities, flight path angle and altitude of the spacecraft

During the simulation run time, the apoapsis could be detected if the altitude of the spacecraft reduced between 2 consecutive timesteps that occur after the periapsis. The altitude of the apoapsis would be recorded as the highest of these 2 consecutive timesteps with a reduction in altitude – which is the first of the 2 timesteps. As the spacecraft starts in a decent, the time of the periapsis can be found as the first time the altitude of the spacecraft increases between 2 consecutive timesteps in the simulation. The simulation terminated after logging an apoapsis, if found.

If the apoapsis is not found, then equation 5-1 was used to find the apoapsis (R_a) based on the final velocities, flight path angle and altitude of the spacecraft. In this scenario it is assumed that, after the simulation has timed out, the spacecraft's trajectory is not influence by anything other than the force due to the gravity of Mars, this mean that it is assumed that the spacecraft is not affected by atmospheric drag or uses any form of propulsion between the end of the simulation and the apoapsis. Equation 5-1 uses Kepler's second law of planetary motion and the conservation of energy (in this case, the sum of kinetic and potential energy as there is no other energy exchange based on the assumption stated) to find the maximum radius form the centre of Mars at which angular

velocity of the spacecraft, relative to the centre of Mars, is equal to the product of the radius form the centre of Mars and the orbital velocity of the spacecraft, which would occur when the spacecraft is traveling perpendicular to the centre of the planet, at the apoapsis (given that the other location that meets this criteria is the periapsis). Equation 5-1 is derived from Curtis [81] and Braeunig [82]

$$R_a = r_1 \, Max \left(\frac{-\left(\frac{2G_c M_{Mars}}{r_1 v_1^2}\right) \pm \sqrt{\left(\frac{2G_c M_{Mars}}{r_1 v_1^2}\right)^2 - 4\left(1 - \left(\frac{2G_c M_{Mars}}{r_1 v_1^2}\right)(-\sin^2 \gamma_1)\right.}}{2\left(1 - \left(\frac{2G_c M_{Mars}}{r_1 v_1^2}\right)\right)} \right) \quad 5\text{-}1$$

Here G_C is the universal gravitational constant, M_{Mars} is the mass of Mars, r_1 is final distance from the centre of Mars to the spacecraft logged by the trajectory model, v_1 is the final velocity of the spacecraft logged by the trajectory model, γ_1 is the final flight path angle of the spacecraft logged by the trajectory model and R_a is the apoapsis distance from the centre of Mars. Spacecraft with trajectories that lead to an apoapsis distance within a target range have been considered to be successfully captured, this target range is discussed in section 3 of this chapter.

The trajectory model was also used to estimate the average heat flux over the surface of the aeroshell, as well as the peak pressure on the aeroshell. As the spacecraft and aeroshell had a fixed mass and design, the ballistic coefficient has an inverse relationship with the radius of the aeroshell, as shown in Eq. 5-2 below.

$$\beta = \frac{M_{AS} + M_{PL}}{C_d \pi a^2} \quad 5\text{-}2$$

Here β is the ballistic coefficient, the mass of the aeroshell and the payload are M_{AS} and M_{PL}, respectively, C_d is the drag coefficient and a is the outer radius of the aeroshell. Aeroshells with higher volumes or larger outer radii must have a lower foam density. The volume of the aeroshell can be calculated as the volume of a cone section, this calculation is shown in Eq. 5-3.

$$V_{AS} = \frac{1}{3}\pi a^2 h \quad 5\text{-}3$$

The relationship between foam density and outer radius can be seen in Eq. 5-4 below.

$$\rho_{Foam} = \frac{M_{AS}}{V_{Cent} + V_{AS}} = \frac{M_{AS}}{V_{Cent} + \frac{1}{3}\pi a^2 h} \quad 5\text{-}4$$

Here V_{Cent} is the volume of foam surrounding the payload in the centre of the spacecraft, h is the thickness of the aeroshell at radius b (see Figure 5-2) and ρ_{Foam} is the density of the foam in use. The relationships described in equations 5-2 and 5-4 show that the ballistic coefficient varies directly with the foam density. Given the material properties also vary with foam density, as described by Gibson and Ashby [30], there must exist a trade off between the material having a density providing a low ballistic coefficient while providing a strong enough material to support the pressure

experienced during the aerocapture and, for a given foam material, a minimum pericentre altitude and average heat flux at which an aerocapture is viable.

To understand if the aeroshell could survive the atmospheric pass, the peak pressure was applied to a plate bending model derived from Bhasker and Varadan [83] for a annular disc with simple supports at the centre. The peak moment and bending stress occurred where the disc met the payload. The peak moment and bending stress were calculated using the equations 5-5 and 5-6, for a given pressure.

$$Mo_{Max} = D_F(1+\nu_{Foam})\left(C_0\left(\frac{4b^2(3+\nu_F)}{1+\nu_F}\right)+C_1\left(2\ln b+\frac{3+\nu_F}{1+\nu_F}\right)+2C_2-C_3\left(\frac{1-\nu_F}{b^2(1+\nu_F)}\right)\right)$$

$$D_F = \frac{E_F h^3}{12(1-\nu_F^2)}$$

$$C_0 = \frac{AP}{32\pi D_F}$$

$$C_1 = -\frac{APa^2}{8\pi D_F} \qquad 5\text{-}5$$

$$C_2 = C_0(4a^2\ln a)+C_3\frac{(1-\nu_F)}{2a^2(1+\nu_F)}$$

$$C_3 = \frac{-4C_0\left(a^2\left(2\ln a-\frac{4D_F}{\kappa G_F h b^2}+2\ln b+1\right)-b^2\right)\left(a^2b^2(1+\nu_F)\right)}{b^2(1-\nu_F)+a^2(1-\nu_F)}$$

$$\sigma_{Max} = \frac{6Mo_{Max}}{h^2} \qquad 5\text{-}6$$

Here Mo is the moment, σ_{Max} is the maximum bending stress, D_F is the disks flexural rigidity, C_0 to C_3 are integral constants, ν_F is Poisson's ratio for the foam material, A is the area of the disc normal to the direction of travel, E is the tensile modulus of the material, G is the bulk modulus of the material, P is the peak dynamic pressure and κ is the shear correction value which is 1 in this case. The shear stress at the joint of between the payload and the aeroshell was also considered using equation 5-7 which has been derived for Megson [84]:

$$\tau_{Max} = \frac{P\,A}{2\pi\,b\,h} = \frac{P\,\pi(a^2-b^2)}{2\pi\,b\,h} = \frac{P(a^2-b^2)}{2\,b\,h} \qquad 5\text{-}7$$

Here the maximum shear force is the product of the peak dynamic pressure (P) and the area of the aeroshell disc that is normal to the direction of travel. The area that the shear load is acting on is the product of the circumference of the payload/ aeroshell joint (2 π b) and the thickness of the aeroshell (h). The factor of safety equation shown in Eq. 4-1 was used to find the factor of safety for the bending stress based on the maximum bending stress found in Eq. 5-6. The shear stress factor of safety was typically two orders of magnitude greater than the bending stress factor of safety. For this reason, a shear failure was not considered to be the limiting factor on the design.

The average dynamic pressure over the surface of the aeroshell, at each timestep, was calculated across the atmospheric transit using equation 5-8 below. This equation was part of the trajectory model, developed by Bailet et al [80].

$$P = \frac{\rho_{Atm} v^2}{2} \qquad 5\text{-}8$$

Here ρ_{Atm} is the atmospheric density and v is the velocity which is found as part of the trajectory model developed by Bailet et al [80].

The average heat flux over the surface of the aeroshell, at each timestep, was calculated across the atmospheric transit using equation 5-9 below which is based on the Sutton Graves equations [85]. This equation was part of the trajectory model, developed by Bailet et al [80].

$$Q = k_{Mars} v^3 \sqrt{\frac{\rho_{Atm}}{a}} \qquad 5\text{-}9$$

Here k_{Mars} is the heat transfer coefficient which is constant for the Martian atmosphere.

Detailed Concept Design

To develop this concept in more detail a direct simulation Monte Carlo analysis of the aeroshell was conducted. This analysis considered the aeroshell while it was traveling at the maximum speed and the minimum altitude found during an aerocapture that would result in the spacecraft arriving in the target orbit. This analysis was conducted by Craig White using the dsmcFoam+ model reported in White et al [79].

5.3 Case Study Parameters

In this case study the following parameters where applied.

Mission Parameters

The initial velocity at the atmospheric entry interface was 5.5 km/s, this is similar to the velocity used by Timmons et al (5.8 km/s) [86] and the Xiuqiang et al (6 km/s) [87]. As discussed in section 2 of this chapter, the initial flight path angle varied across a range, with the limits of that range being between 2° and 8° downward. This range was selected based on trial and error after finding that lower flight path angles would result in spacecraft that crashed and higher angles resulted in spacecraft failing to meet the apoapsis range requirements. The target captured apoapsis distance from the centre of Mars was between 30,000 and 40,000 km, this range was thought to be a useful range as it is around the same altitude as the Emirates Mars Mission – apoapsis of 40000 km as reported by Amiri et al [88]. The total mission mass was 12.5 tonnes, of which the aeroshell had a mass of 2.5 tonnes and the payload had a mass of 10 tonnes, this value was selected as it to provide a large satellite as the payload of around the same scale as the Hubble telescope [89]. The payload had a radius of 3 m and a length of 5 m and a foam wall of 0.5 m on top of that. The aeroshell root thickness was 1 m. The mass of Mars was 6.417×10^{23} kg which is within the range reported by Null [90] based in the Mariner IV mission. The gravitational constant was 6.674×10^{-11} m^3 kg^{-1} s^{-2} as

reported by Mohr et al [91]. A coefficient of drag of 2 was used and a lift coefficient of 0 was used assuming that there was little to no lift generated by this shape.

Material Parameters

The material envisioned for the aeroshell was a solid foam made of PEEK with closed cells. As discussed, the final material properties were derived using the Gibson Ashby [30] equations, the raw material properties for the PEEK material are shown in Table 5-1 below.

Table 5-1 – Foam base material properties

Property	Value
Density, ρ (kg/m^3)	1440
Tensile Yield Strength, σ_{Yeild} (N/m^2)	$196x10^6$
Shear Yield Strength, τ_{Yeild} (N/m^2)	$72x10^6$
Elastic Modulus, E (N/m^2)	$12x10^2$

A Poisson's ratio of 0.3 was used for the foam.

5.4 Results

In Figure 5-3 the ballistic coefficient of the spacecraft is compared with both the peak heat flux and minimum mechanical factor of safety experienced for both the lowest initial flight path angle that was successful to the highest flight path angle required to meet the captured orbit, for the range of trajectories that where successfully captured into the target orbit. The ballistic coefficient has been calculated using Eq. 5-2 based on the cross-sectional area of the aeroshell and the mission mass. The peak heat flux has been calculated using the outputs of the trajectory model, developed by Bailet et al [80], and Eq. 5-9. The mechanical stress was calculated using the outputs of the trajectory model, developed by Bailet et al [80] and Eq. 5-8, the material properties used here were estimated using the Gibson Ashby equations [30] and the density of foam used for that aeroshell. The range of results are only for the mission that successfully meet the target apoapsis range from the "lowest" initial flight path angle that was successful to the "highest" flight path angle that was successfully.

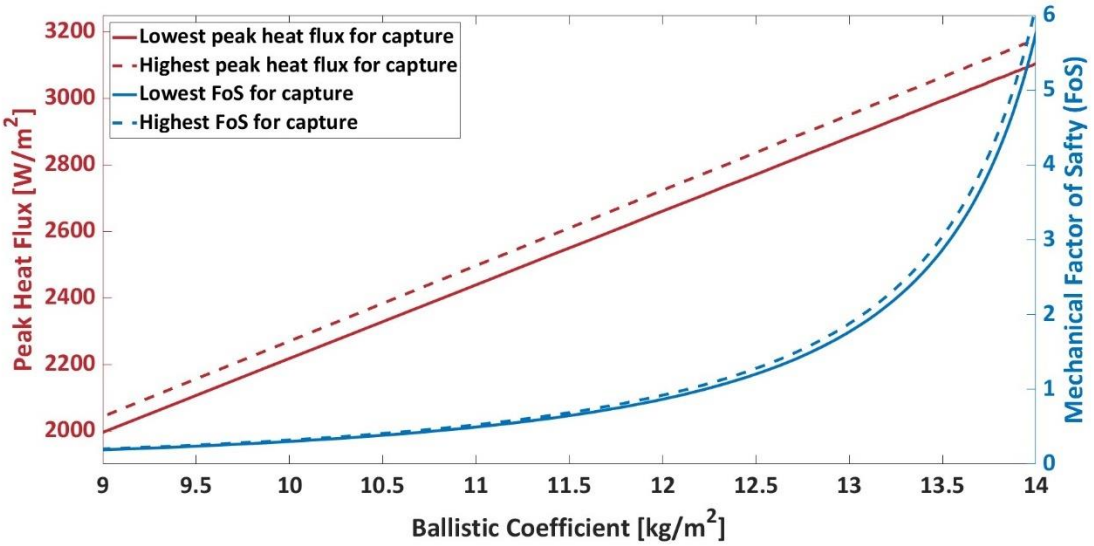

Figure 5-3 – Ballistic coefficient compared against foam aeroshell mechanical factor of safety and average heat flux across the velocity facing surface, as discussed this figure used a trajectory model developed by Gilles Bailet [80],

For the detailed study, the lowest ballistic coefficient that could achieve a safe aerocapture transfer was selected. This would be a spacecraft with a ballistic coefficient of 12 kg/m^2 and an outside diameter of 25.5 m (i.e. a = 12.75m). This would require a foam with a density of 86 kg/m^3. This spacecraft reached its minimum altitude at 91 km, at which point it had a velocity of 5.16 km/s. At this ballistic coefficient, the peak heat flux estimated by the trajectory model, developed by Gilles Bailet [80], is 2693 W/m^2 and the peak dynamic pressure is 71 N/m^2.

The parameters above were used by White for the DSMC analysis, the results shown are the outcomes of his work. Figure 5-4 below shows a 2D map of the translational temperature of the atmosphere around the spacecraft found using the DSMC analysis at the spacecraft's minimum altitude.

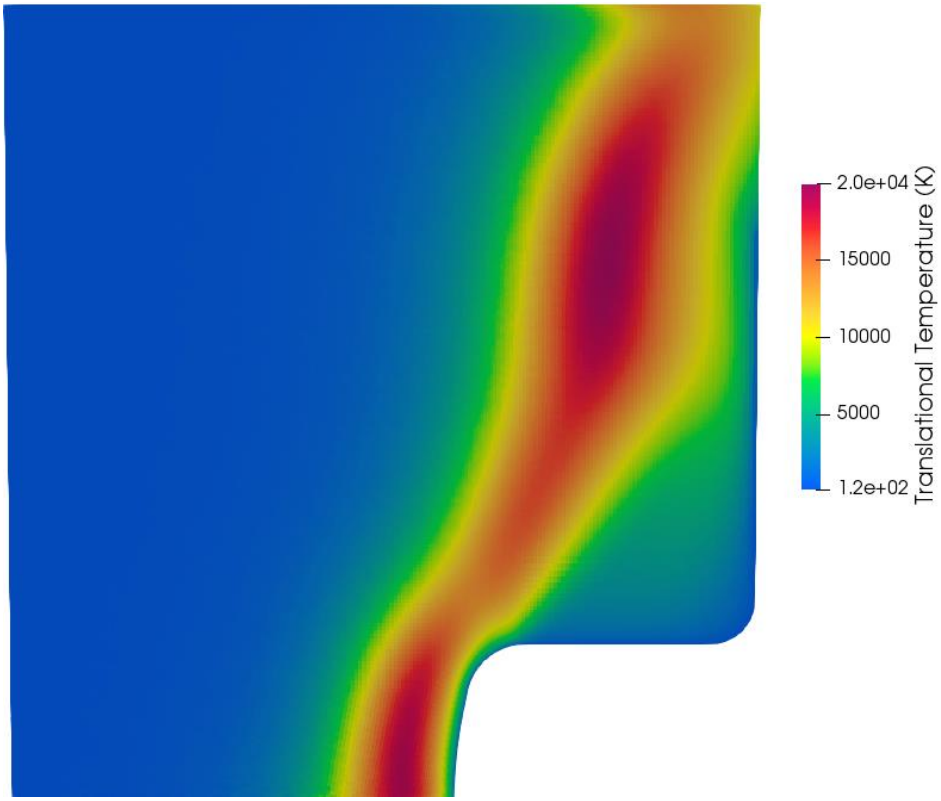

Figure 5-4 – 2D plot of atmospheric translational temperature close to a solid foam aeroshell while the spacecraft is at its periapsis presented in [11] and generated by C White

Figure 5-5 below shows both the heat flux experienced on the surface of the aeroshell and the pressure of the atmosphere around the aeroshell using the DSMC analysis for the minimum altitude condition.

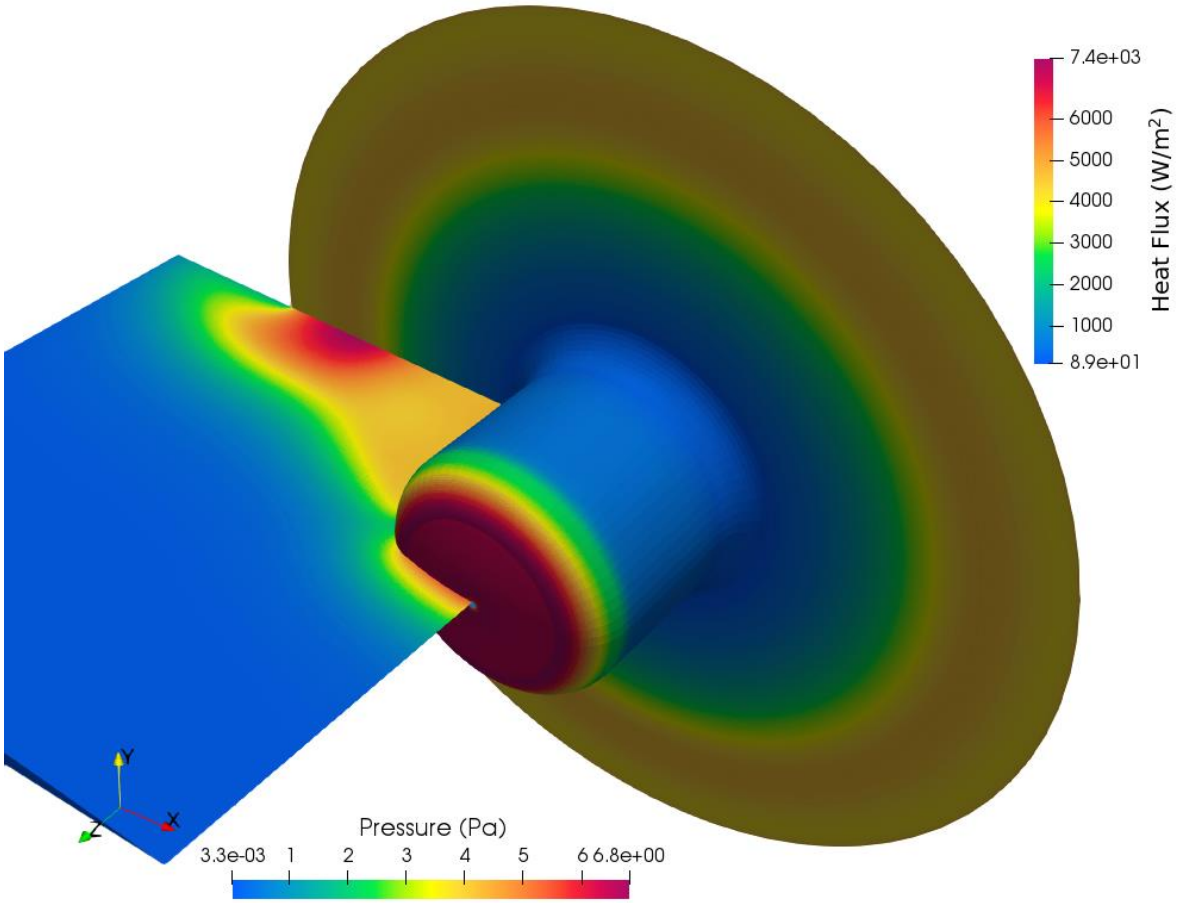

Figure 5-5 – 3D plot of the surface heat flux on the surface of a foam aeroshell and 2D plot of the atmospheric pressure close to the foam aeroshell while the spacecraft is at its periapsis. The figure was generated by C White as part of the work for [10] although not presented there.

5.5 Discussion

It can be seen in Figure 5-3, that both the heat flux experienced by the surface of the aeroshell and the factor of safety of the aeroshell vary directly with the ballistic coefficient. This is as expected, as a higher ballistic coefficient would result in lower atmospheric passes and so a higher heat flux, while at the same time a lower ballistic coefficient would be the result of a high-density foam with a higher material strength, as well as a longer deceleration period so a lower pressure load. This result – that an aeroshell with a low ballistic coefficient experiences less heat flux during an aerocapture manoeuvre than an aeroshell with a higher ballistic coefficient would for an aerocapture manoeuvre with the same change in velocity – is also predicted in literature. For example, this affect is part of the rationale behind the used of the Hypersonic Inflatable Aerodynamic Decelerator (HIAD) described by Dwyer Cianciolo et al [78].

The detailed results from the DSMC model show a similar average heat flux, as was predicted by the trajectory model, with both showing an average heat flux between 2 kW/m^2 and 3 kW/m^2. However, the peak heat flux found in the DSMC model is considerably higher than that predicted by the trajectory model with an increase of around three times the average value. This result was

expected when the shape of the aeroshell is considered with its protruding centre. The average pressure reported by the DSMC model is significantly lower than the average pressure predicted by the trajectory model. The DSMC model reports a peak pressure across the surface of 6.8 Pa, at the periapsis, which is less than the average dynamic pressure across the surface reported by the trajectory model, at the periapsis, which found an average pressure across the surface of 71 Pa for a spacecraft, with the same ballistic coefficient, surface area, and speed. This result is somewhat surprising, and may indicate that the model used to predict the dynamic pressure, as part of the trajectory model, does not accurately predict surface pressure in low pressure environments with a complex shape. If the result in the DSMC is correct and aligns with the dynamic pressure on the surface of the aeroshell, then a more detailed model of the trajectory of the spacecraft may be required. The result of the DSMC suggests that a thermal protection system may be required on the nose of the spacecraft where the heat flux is highest.

The performance of the foam aeroshell can be compared with the performance of other aeroshells and an equivalent chemical engine. The Hypersonic Inflatable Aerodynamic Decelerator (HIAD) proposed by Dwyer Cianciolo et al [78] has been used for the comparison in Table 5-2 below. In the comparison in Table 5-2, the chemical propulsion capture provides the same change in velocity as the aerocapture manoeuvres with an engine that has a specific impulse of 370 s which is based on the propulsion system example presented by Dwyer Cianciolo et al [78].

Table 5-2 – Capture manoeuvre hardware comparison table

System Used for Capture	Foam Aeroshell	HIAD (Ø23m)	Chemical Propulsion
Mission Specification	12.5 tonne mission Aeroshell Ø25.5 m	109 tonne mission Aeroshell Ø23 m	12.5 tonne mission Engine I_{sp} 370 s
Capture Hardware Percent of Mission's Mass	20%	25%	40%
Storage Volume	3 m^3	120 m^3	11 m^3
Ballistic Coefficient	12 kg/m^2	135 kg/m^2	N/A
Heritage	None	Demonstrated in [92]	Extensive Heritage

The comparison in Table 5-2 shows that a foam printed aeroshell could achieve lower mission mass percentage than a HIAD system or a conventional chemical propulsion manoeuvre if the design presented can survive the thermal and mechanical loads discussed. It should be noted that the mission that considers the use of a HIAD has a mass that is an order of magnitude greater than that of the solid foam example mission mass.

The high heat flux shown around the nose in the DSMC analysis suggests that the foam aeroshell would most likely need further thermal protection on the nose section of the aeroshell. Additional, thermal protection in this area would result in the mass of the aeroshell increasing, but this case has not been considered in this study.

While the final diameter selected for the solid foam aeroshell (25.5 m) is less than the 100 m span threshold for large-scale structures, the result is still of relevance to the broader study of large-scale space structures. The volume of the aeroshell is more than 170 m^3, this print volume could be used to make a slender structure that meet the 100 m span threshold and so provides some detail on the practicalities of manufacturing such a large structure, for example storage volume and mass. The analysis also considered larger structures with lower ballistic coefficients some of which met the 100 m threshold. These large scale aeroshells showed a further reduction in in heat flux but would have required stronger materials to survive the stress associated with the high deceleration.

5.6 Limitations of the Research

This study considered a conceptual evaluation of solid foam aeroshells, and to do this some assumptions and simplifications were made. Further research could provide a deeper understanding of the design requirements of a foam aeroshell system which could help evaluate the feasibility of the design. While the plate theory model of the foam aeroshell may be suitable for an initial concept design, a more accurate finite element analysis of the selected design could provide a much deeper understanding of the thermal and mechanical suitability.

As has been discussed, the mission mass and base material for the foam were fixed. Further study could be conducted to understand the impact of varying these constraints and this may have allowed for a direct comparison to the HIAD system.

The material properties for the foam material suggested, a PEEK base solid foam, was estimated using the Gibson Ashby approximations. While this allows for a quick comparison of foams of various densities, a more accurate approach would have been to directly measure the material properties of the foam via testing. Additionally, no limits were placed on the density of foam used when in practise there should be a lower limit for foam density of a material. Further research into the material manufacturing process would be required to understand the limit of a PEEK based solid foam.

As discussed, the finalised aeroshell requires additional thermal protection around the nose, but this is not considered in the study. A thermal protection system like this would add additional mass to the mission and so impact the ballistic coefficient and hence the trajectory. Further research could be carried out to explore what this thermal protection could consist of and how it would impact the mission and aeroshell design.

This study only considered aeroshells for use in an aerocapture manoeuvre around Mars, but it is possible that a solid foam aeroshell could be used for other application such as de-orbiting as suggested in the REDEMPTION mission [35]. Further study could be conducted to consider aerocaptures and deorbiting of missions into atmospheres that are not Martian.

This study only considers one shape of aeroshell. Given that one of the key advantages of an ISM system is its adaptability, further research into the use of novel shapes constructed using ISM solid foams could be considered.

6. Conclusions and Future Work

6.1 Conclusions

Chapter 1 set out the motivation for developing an in-space manufacturing facility that is capable of producing large-scale space structures. A key advantage of in-space manufacturing is the possibility of removing the many of the factors that limit the size of space infrastructure. This could enable larger scale space structures such as the one considered by Huebner et al in the OSAM-2 mission [6], McInnes et al as a reflector to harvest an M-type asteroid [25] or Fraas as an orbital reflector [26]. In chapter 2 of this thesis, a literature review of current developments in the field of in-space manufacturing and solid foam manufacturing is presented. This review shows that, while there has been an increased interest in in-space manufacturing in recent years [19] and there has demonstration of the capability to manufacture components in space (such as the 3D printing carried out on the ISS reported by Prater et al [14]), there are several key developments that would be required before a fully automated in-space manufacturing facility would be capable of constructing large-scale space structures namely:

- Demonstrating systems capable of continuous printing while in orbit,
- Demonstrating systems capable of manufacturing parts while in vacuum (Prater et al reported on a print inside the ISS [14]

Chapter 2 also considered literature concerning solid foams, their manufacturing processes, their structure and methods of predicting their material properties. Both solid foams and cellular solids have been used in terrestrial and space applications. While there have been no in-space demonstrations of solid foam manufacturing, there has been development towards this in the REDEMPTION mission as reported by Valdatta et al [35], with demonstration of solid foam manufacturing in vacuum.

In chapter 3, solid foams were compared with other technologies that have been considered for ISM. As is discussed in section 7 of chapter 3, the solid foams show a particular advantage for rapid construction due to their high volumetric print rate. However, the poor material quality and relatively weak mechanical strength means that they are less favourable for high precision or long-term construction in space.

In chapters 4 and 5, solid foams were considered for use in detailed case studies, with chapter 4 considering two generalised cases and comparing solid foams to other ISM processes and materials, whereas chapter 5 considered a specific case, with solid foams compared with an inflatable system. In chapter 4, solid foams and a solid foam manufacturing process were shown to have significant advantages in construction energy and overall construction time. Chapter 5 considered solid foams being used to construct an aeroshell and is compared with both a HIAD system and a chemical propulsion system. It was shown that it may be possible to construct a solid foam aeroshell system with a similar proportion of mission mass as the HIAD system proposed by Dwyer Cianciolo et al [78].

6.2 Future work

While chapters 3, 4 and 5 show that there are potential advantages in using solid foams for in-space manufacturing, there are still key gaps in the understanding of the use of solid foams in space:

- Applied material properties and quality for solid foams made in space.
- Process characteristics

Future exploration of these topics would further develop the use of solid foams for ISM.

6.2.1 Material properties

While there are models used to predict the properties of solid foams, notable the Gibson Ashby model [30], these models have been shown to have a significant margin of error when compared with empirical results, as discussed by Fisher et al [38]. Both the final solid foam material properties and the consistency of the material properties are critical to the performance of the foam materials discussed in chapter 4 and 5. As such, understanding the relationship between foam solid factor, the base material properties and the manufacturing process with the final mechanical properties for a solid foam is critical to understand how to apply solid foams for ISM. There are two approaches to understanding the material properties of solid foams produced in vacuum.

1. Empirical measurements
2. Computational modelling

Mechanical strength measurements of solid foams made in space, with various solid fraction and base materials, could be used to understanding how the applied mechanics properties of a solid foam produced in space vary with both solid fraction and base material. Ideally such a test would be carried out in-orbit while in vacuum to provide a close representation of the application environment, however practically this would be difficult to arrange. It may be more practical to consider mechanical testing of these solid foams made in vacuum and/or made in freefall. An in-vacuum test could be conducted in the laboratory with access to a vacuum chamber and mechanical test equipment such as a tensile test or bending test.

In addition to and alongside empirical testing, a computational model could be used to understand how the solid foam mesostructured develops in vacuum, for a given solid fraction and base material. Further computational modelling could be used to predict the mechanical properties of the solid foams based on their mesostructured and solid material using FEA in a similar method as is presented in Fischer et al [38]. The results of the computational analysis could be compared to the empirical results to evaluate their suitability where possible.

6.2.2 Process Demonstration and Characteristics

Throughout this thesis, process characteristics, such as the print rates and the power consumption, have been presented based on terrestrial examples. Given the significance of these characteristics in the results presented in chapter 4, a better understanding of these process characteristics could be

key to verifying the possible opportunities presented by manufacturing solid foams in space. To understand these process characteristics, a demonstration model of a foam 3D printer could be constructed and tested. The printer would be similar to the foam 3D printer demonstration by Barnett and Gosselin [50], but capable of operation in vacuum. Such a demonstration model would allow for the direct measurement of the power consumption and print rates using a test set up similar to the Hassan et al [72] carried out on a FDM printer. This demonstration foam 3D printer could also be used to produce the mechanical test samples discussed in section 6.1.1 of this chapter.

References

[1] I. D. Boyd, R. S. Buenconsejo, D. Piskorz, B. Lal, K. W. Crane, and E. De La Rosa Blanco, 'On-Orbit Manufacturing and Assembly of Spacecraft', The Institute for Defence Analyses, Washington DC, IDA Paper P-8335, Jan. 2017. [Online]. Available: https://www.ida.org/-/media/feature/publications/o/on/on-orbit-manufacturing-and-assembly-of-spacecraft/on-orbit-manufacturing-and-assembly-of-spacecraft.ashx

[2] 'Artemis - NASA'. Accessed: Aug. 11, 2024. [Online]. Available: https://www.nasa.gov/humans-in-space/artemis/

[3] 'Asteroid Mining Corporation', Asteroid Mining Corporation. Accessed: Aug. 11, 2024. [Online]. Available: https://www.asteroidminingcorporation.co.uk

[4] NASA, 'International Space Station Facts and Figures - NASA'. Accessed: Aug. 24, 2025. [Online]. Available: https://www.nasa.gov/international-space-station/space-station-facts-and-figures/

[5] ESA-ESTEC, *ECSS-Q-ST-70-01C – Cleanliness and contamination control (15 November 2008) | European Cooperation for Space Standardization*, ESTEC, P.O. Box 299, 2200 AG Noordwijk, The Netherlands., Nov. 15, 2008. Accessed: Apr. 07, 2024. [Online]. Available: https://ecss.nl/standard/ecss-q-st-70-01c-cleanliness-and-contamination-control/

[6] L. D. Huebner, P. Shestople, S. Patané, and D. Hillsberry, 'OSAM-2: Plans and Progress for the First Demonstration of Structural Manufacturing in Space', Accessed: Aug. 13, 2024. [Online]. Available: https://ntrs.nasa.gov/citations/20220007646

[7] M. Molitch-Hou, 'Overview of additive manufacturing process', in *Additive Manufacturing*, J. Zhang and Y.-G. Jung, Eds., Butterworth-Heinemann, 2018, pp. 1–38. doi: 10.1016/B978-0-12-812155-9.00001-3.

[8] S. M. Thompson, L. Bian, N. Shamsaei, and A. Yadollahi, 'An overview of Direct Laser Deposition for additive manufacturing; Part I: Transport phenomena, modeling and diagnostics', *Additive Manufacturing*, vol. 8, pp. 36–62, 2015.

[9] W. E. Frazier, 'Metal Additive Manufacturing: A Review', *J. of Materi Eng and Perform*, vol. 23, no. 6, pp. 1917–1928, Jun. 2014, doi: 10.1007/s11665-014-0958-z.

[10] Peter G.B. Hastie, Gilles Bailet, and Colin R. McInnes, 'On-Orbit Manufacturing of Large Space Structures Using Solid Foams', in *IAF MATERIALS AND STRUCTURES SYMPOSIUM*, UAE: International Astronmautical Federation, Oct. 2021. Accessed: Apr. 13, 2024. [Online]. Available: https://iafastro.directory/iac/paper/id/63981/summary/

[11] P. Hastie, G. Bailet, C. White, and C. R. McInnes, 'The Use of In-Space Manufactured Solid Foams for Aerocapture', presented at the 18th International Planetary Probe Workshop, 2021. Accessed: Aug. 26, 2021. [Online]. Available: https://drive.google.com/file/d/16jTDSiqqslnTxWTPcBx4QBqwFq_JKTIL/edit

[12] J. R. Wertz and W. Larson, *Space Mission Analysis and Design*, 3rd ed. in Space Technology Library. Springer Netherlands, 1999. Accessed: Apr. 15, 2021. [Online]. Available: https://www.springer.com/gp/book/9780792359012

[13] M. E. Lippman, 'In-space fabrication of thin-film structures', Astro Research Corporation, Santa Barbara, California, NASA Contractor Report NASA CR-1969, Feb. 1972. [Online]. Available: https://ntrs.nasa.gov/citations/19720009888

[14] T. Prater, N. Werkheiser, F. Ledbetter, D. Timucin, K. Wheeler, and M. Snyder, '3D Printing in Zero G Technology Demonstration Mission: complete experimental results and summary of related material modeling efforts', *Int J Adv Manuf Technol*, vol. 101, no. 1, pp. 391–417, Mar. 2019, doi: 10.1007/s00170-018-2827-7.

[15] D. Alexander and N. Murphy, 'Payload Design and Sizing', in *The International Handbook of Space Technology*, M. Macdonald and V. Badescu, Eds., in Springer Praxis Books. , Berlin, Heidelberg: Springer, 2014, pp. 117–142. doi: 10.1007/978-3-642-41101-4_6.

[16] M. R. Patel, 'Electrical Power', in *The International Handbook of Space Technology*, M. Macdonald and V. Badescu, Eds., in Springer Praxis Books. , Berlin, Heidelberg: Springer, 2014, pp. 249–277. doi: 10.1007/978-3-642-41101-4_10.

[17] D. R. Williams, 'NSSDCA/COSPAR ID: 1969-085A', NASA Space Science Dara Coordinated Archive. [Online]. Available: https://nssdc.gsfc.nasa.gov/nmc/spacecraft/display.action?id=1969-085A

[18] T. A. Siewert, R. W. Heine, C. M. Adams, and J. R. Williams, 'The Skylab Brazing Experiment', *WJRS*, pp. 291–300, Oct. 1977.

[19] R. Skomorohov, 'In-orbit spacecraft manufacturing: near-term business cases', International Space University, Illkirch-Graffenstaden, 2016.

[20] ESA, 'POP3D printer'. Accessed: Apr. 26, 2021. [Online]. Available: http://www.esa.int/ESA_Multimedia/Images/2014/11/POP3D_printer

[21] E. A. Slejko, N. Sesto Gorella, A. Makaya, P. Gallina, N. Scuor, and S. Seriani, 'Vacuum 3D printing of highly filled polymeric matrix composites', *Acta Astronautica*, vol. 204, pp. 25–33, Mar. 2023, doi: 10.1016/j.actaastro.2022.12.033.

[22] S. Litkenhous, 'In-Space Manufacturing', NASA. Accessed: Apr. 15, 2021. [Online]. Available: http://www.nasa.gov/oem/inspacemanufacturing

[23] 'Spaceflight Missions', Made In Space. Accessed: Apr. 15, 2021. [Online]. Available: https://madeinspace.us/spaceflight-missions/

[24] R. P. Hoyt, J. Cushing, G. Jimmerson, J. Slostad, R. Dyer, and S. Alvarado, 'SpiderFab: Process for on-orbit construction of kilometer-scale apertures', Tethers Unlimited, Inc, Bothell, Washington, USA, Final Report HQ-E-DAA-TN62833, Nov. 2018. [Online]. Available: https://ntrs.nasa.gov/citations/20190001156

[25] C. McInnes, 'Harvesting Near Earth Asteroid Resources Using Solar Sail Technology', in *Fourth International Symposium on Solar Sailing*, Kyoto, Japan, Jan. 2017, p. 6. Accessed: Apr. 16, 2021. [Online]. Available: http://eprints.gla.ac.uk/135798/

[26] L. Fraas, 'Sunbeams From Mirrors In Dawn-Dusk Orbit For Earth Solar Power Fields', in *CPV-9*, in AIP Conf., vol. 1556. Miyazaki, Japan: International Astronautical Federation, Sep. 2013, pp. 234–238. doi: 10.1063/1.4822239.

[27] J. Y. Wong and A. C. Pfahnl, '3D Printing of Surgical Instruments for Long-Duration Space Missions', *Aviation, Space, and Environmental Medicine*, vol. 85, no. 7, pp. 758–763, Jul. 2014, doi: 10.3357/ASEM.3898.2014.

[28] 'Fiber Optics', Made In Space. Accessed: Apr. 26, 2021. [Online]. Available: https://madeinspace.us/capabilities-and-technology/fiber-optics/

[29] A. Baptista, F. J. G. Silva, J. Porteiro, J. L. Míguez, G. Pinto, and L. Fernandes, 'On the Physical Vapour Deposition (PVD): Evolution of Magnetron Sputtering Processes for Industrial Applications', *Procedia Manufacturing*, vol. 17, pp. 746–757, Jan. 2018, doi: 10.1016/j.promfg.2018.10.125.

[30] L. J. Gibson and M. F. Ashby, *Cellular solids: structure and properties*, 2nd ed. in Cambridge solid state science series. Cambridge: Cambridge University Press, 1997.

[31] M. F. Ashby, A. G. Evans, N. A. Fleck, L. J. Gibson, J. W. Hutchinson, and H. N. G. Wadley, *Metal Foams: A Design Guide*. London: Butterworth-Heinemann, 2000.

[32] W. Drenckhan and S. Hutzler, 'Structure and energy of liquid foams', *Advances in Colloid and Interface Science*, vol. 224, pp. 1–16, Oct. 2015, doi: 10.1016/j.cis.2015.05.004.

[33] S. Hilgenfeldt, A. M. Kraynik, D. A. Reinelt, and J. M. Sullivan, 'The structure of foam cells: Isotropic Plateau polyhedra', *Europhysics Letters*, vol. 67, no. 3, pp. 484–490, 2004, doi: 10.1209/epl/i2003-10295-7.

[34] A. Hajimohammadi, T. Ngo, P. Mendis, and J. Sanjayan, 'Regulating the chemical foaming reaction to control the porosity of geopolymer foams', *Materials & Design*, vol. 120, pp. 255–265, Apr. 2017, doi: 10.1016/j.matdes.2017.02.026.

[35] M. Valdatta *et al.*, 'Inflatable System Based on Polyurethanic Foam', presented at the 63rd International Astronautical Congress, Naples, Italy: IAF, Jan. 2013, pp. 153–160.

[36] S. Schlögl, M. Reischl, V. Ribitsch, and W. Kern, 'UV induced microcellular foaming—A new approach towards the production of 3D structures in offset printing techniques', *Progress in Organic Coatings*, vol. 73, no. 1, pp. 54–61, Jan. 2012, doi: 10.1016/j.porgcoat.2011.08.020.

[37] J. Banhart, 'Manufacture, characterisation and application of cellular metals and metal foams', *Progress in Materials Science*, vol. 46, no. 6, pp. 559–632, Jan. 2001, doi: 10.1016/S0079-6425(00)00002-5.

[38] F. Fischer, G. T. Lim, U. A. Handge, and V. Altstädt, 'Numerical Simulation of Mechanical Properties of Cellular Materials Using Computed Tomography Analysis', *Journal of Cellular Plastics*, vol. 45, no. 5, pp. 441–460, Sep. 2009, doi: 10.1177/0021955X09339340.

[39] F. Garcia-Moreno, M. Mukherjee, C. Jimenez, and J. Banhart, 'X-ray radioscopy of liquid metal foams under microgravity', *Trans Indian Inst Met*, vol. 62, no. 4, pp. 451–454, Oct. 2009, doi: 10.1007/s12666-009-0084-z.

[40] F. Quadrini, G. M. Tedde, L. Santo, and J. J. W. A. van Loon, 'Solid-state foaming of epoxy resin under hypergravity and simulated microgravity', *Advances in Polymer Technology*, vol. 37, no. 7, pp. 2616–2624, 2018, doi: https://doi.org/10.1002/adv.21937.

[41] D. Langevin and M. Vignes-Adler, 'Microgravity studies of aqueous wet foams', *Eur. Phys. J. E*, vol. 37, no. 3, p. 16, Mar. 2014, doi: 10.1140/epje/i2014-14016-3.

[42] B. M. Somosvári, P. Bárczy, J. Szóke, P. Szirovicza, and T. Bárczy, 'FOCUS: Foam evolution and stability in microgravity', *Colloids and Surfaces A: Physicochemical and Engineering Aspects*, vol. 382, no. 1, pp. 58–63, Jun. 2011, doi: 10.1016/j.colsurfa.2011.01.035.

[43] N. Gerdes *et al.*, 'Selective Laser Melting for processing of regolith in support of a lunar base', *Journal of Laser Applications*, vol. 30, no. 3, p. 032018, Aug. 2018, doi: 10.2351/1.5018576.

[44] S. L. Taylor *et al.*, 'Sintering of micro-trusses created by extrusion-3D-printing of lunar regolith inks', *Acta Astronautica*, vol. 143, pp. 1–8, Feb. 2018, doi: 10.1016/j.actaastro.2017.11.005.

[45] C. Buchner, R. H. Pawelke, T. Schlauf, A. Reissner, and A. Makaya, 'A new planetary structure fabrication process using phosphoric acid', *Acta Astronautica*, vol. 143, pp. 272–284, Feb. 2018, doi: 10.1016/j.actaastro.2017.11.045.

[46] A. Mariappan, V. R. S. Kumar, S. J. Weddell, V. A. Muruganandan, and I.-S. Jeung, 'Theoretical studies on space debris recycling and energy conversion system in the International Space Station', *Engineering Reports*, vol. 3, no. 5, p. e12317, 2021, doi: 10.1002/eng2.12317.

[47] K. Lietaert *et al.*, 'Meteorite as raw material for Direct Metal Printing: A proof of concept study', *Acta Astronautica*, vol. 143, pp. 76–81, Feb. 2018, doi: 10.1016/j.actaastro.2017.11.027.

[48] A. Ohndorf, S. Eberle, T. Uhlig, R. Faller, M. Schmidhuber, and R. Ballweg, 'Mission Operations', in *Spacecraft Operations*, T. Uhlig, F. Sellmaier, and M. Schmidhuber, Eds., Vienna: Springer, 2015, pp. 35–89. doi: 10.1007/978-3-7091-1803-0_2.

[49] ESA-ESTEC, *ECSS-E-ST-10C Rev.1 – System engineering general requirements (15 February 2017) | European Cooperation for Space Standardization*, ESTEC, P.O. Box 299, 2200 AG Noordwijk, The Netherlands. doi: 15/02/2017.

[50] E. Barnett and C. Gosselin, 'Large-scale 3D printing with a cable-suspended robot', *Additive Manufacturing*, vol. 7, pp. 27–44, Jul. 2015, doi: 10.1016/j.addma.2015.05.001.

[51] Y. Li and Y. Lou, 'Tensile and Bending Strength Improvements in PEEK Parts Using Fused Deposition Modelling 3D Printing Considering Multi-Factor Coupling', *Polymers*, vol. 12, no. 11, Art. no. 11, Nov. 2020, doi: 10.3390/polym12112497.

[52] 'Apium PEEK 450', Apium. Accessed: Aug. 17, 2024. [Online]. Available: https://apiumtec.com/en/apium-shop-en/apium-peek-450-filament

[53] K. Zhang, S. Wang, W. Liu, and X. Shang, 'Characterization of stainless steel parts by Laser Metal Deposition Shaping', *Materials & Design*, vol. 55, pp. 104–119, Mar. 2014, doi: 10.1016/j.matdes.2013.09.006.

[54] M. Yakout, M. A. Elbestawi, and S. C. Veldhuis, 'Density and mechanical properties in selective laser melting of Invar 36 and stainless steel 316L', *Journal of Materials Processing Technology*, vol. 266, pp. 397–420, Apr. 2019, doi: 10.1016/j.jmatprotec.2018.11.006.

[55] S. Mengali *et al.*, 'FIRST SURFACE FLEXIBLE OPTICAL SOLAR REFLECTORS WITH INTERFERENTIAL CERMET COATINGS', 2018. Accessed: Oct. 19, 2024. [Online]. Available: https://www.semanticscholar.org/paper/FIRST-SURFACE-FLEXIBLE-OPTICAL-SOLAR-REFLECTORS-Mengali-Simeoni/7b4d6e7f1e7ca4095cc3f0eda8305e7fac2ea865

[56] D. G. Gilmore, Ed., *Spacecraft Thermal Control Handbook*, Second., vol. 1. El Segundo, California: The Aerospace Press, 2002. Accessed: Apr. 15, 2021. [Online]. Available: https://www.academia.edu/934756/Thermal_Control_Handbook

[57] Z. Zhang, R. Wang, T. Hao, C. Guo, D. Xue, and X. Zhang, 'Fabrication of a high-accuracy phase-type computer-generated hologram by physical vapor deposition', *Appl. Opt., AO*, vol. 57, no. 34, pp. F31–F36, Dec. 2018, doi: 10.1364/AO.57.000F31.

[58] J. E. Fesmire, B. E. Coffman, B. J. Meneghelli, and K. W. Heckle, 'Spray-on foam insulations for launch vehicle cryogenic tanks', *Cryogenics*, vol. 52, no. 4, pp. 251–261, Apr. 2012, doi: 10.1016/j.cryogenics.2012.01.018.

[59] X. Xiaodai, W. Sixian, C. Chen, W. Junjie, and Z. Yuan, 'Thermal performance study for hybrid SOFI and MLI system used in space', *AIP Conference Proceedings*, vol. 1573, no. 1, pp. 716–719, Jan. 2014, doi: 10.1063/1.4860773.

[60] T. Keller, C. Haas, and T. Vallée, 'Structural Concept, Design, and Experimental Verification of a Glass Fiber-Reinforced Polymer Sandwich Roof Structure', *Journal of Composites for Construction*, vol. 12, no. 4, pp. 454–468, Aug. 2008, doi: 10.1061/(ASCE)1090-0268(2008)12:4(454).

[61] Space Exploration Technologies Corp, 'Falcon 9: Capabilities and Services'. Space Exploration Technologies Corp (SpaceX), Jan. 2024. [Online]. Available: https://www.spacex.com/media/Capabilities&Services.pdf

[62] Y. Sun, L. Li, and D. Tiniakov, 'Introduction', in *Reliability Engineering*, Y. Sun, L. Li, and D. Tiniakov, Eds., Singapore: Springer Nature, 2024, pp. 1–25. doi: 10.1007/978-981-99-5978-5_1.

[63] O. B. Toon, C. P. McKay, R. Courtin, and T. P. Ackerman, 'Methane rain on Titan', *Icarus*, vol. 75, no. 2, pp. 255–284, Aug. 1988, doi: 10.1016/0019-1035(88)90005-X.

[64] S. Pugh, *Total design: integrated methods for successful product engineering*. Wokingham: Addison-Wesley, 1991. [Online]. Available: https://go.exlibris.link/GWHD8rBw

[65] T. H. G. Megson, 'Chapter 9 - Bending of Beams', in *Structural and Stress Analysis (Second Edition)*, T. H. G. Megson, Ed., Oxford: Butterworth-Heinemann, 2005, pp. 209–249. doi: 10.1016/B978-075066221-5/50010-2.

[66] T. H. G. Megson, Ed., 'Appendix A - Table of Section Properties', in *Structural and Stress Analysis (Second Edition)*, Oxford: Butterworth-Heinemann, 2005, pp. 713–714. doi: 10.1016/B978-075066221-5/50023-0.

[67] D. Sleight and D. Muheim, 'Parametric Studies of Square Solar Sails Using Finite Element Analysis', in *45th AIAA/ASME/ASCE/AHS/ASC Structures, Structural Dynamics & Materials Conference*, Palm Springs, California: American Institute of Aeronautics and Astronautics, Apr. 2004. doi: 10.2514/6.2004-1509.

[68] C. Balaji, B. Srinivasan, and S. Gedupudi, 'Chapter 8 - thermal radiation', in *Heat transfer engineering*, C. Balaji, B. Srinivasan, and S. Gedupudi, Eds., Academic Press, 2021, pp. 233–294. doi: https://doi.org/10.1016/B978-0-12-818503-2.00008-3.

[69] C. Balaji, B. Srinivasan, and S. Gedupudi, 'Chapter 2 - One-dimensional, steady state heat conduction', in *Heat transfer engineering*, C. Balaji, B. Srinivasan, and S. Gedupudi, Eds., Academic Press, 2021, pp. 15–64. doi: https://doi.org/10.1016/B978-0-12-818503-2.00002-2.

[70] Z. Horak, K. Dvorak, L. Zarybnicka, H. Vojackova, J. Dvorakova, and M. Vilimek, 'Experimental Measurements of Mechanical Properties of PUR Foam Used for Testing Medical Devices and Instruments Depending on Temperature, Density and Strain Rate', *Materials*, vol. 13, no. 20, Art. no. 20, Jan. 2020, doi: 10.3390/ma13204560.

[71] Victrex plc, 'Victrex™ PEEK 450G™'. Nov. 2019. [Online]. Available: http://www.victrex.com/

[72] M. Hassan, H. W. Jeon, G. Kim, and K. Park, 'The effects of infill patterns and infill percentages on energy consumption in fused filament fabrication using CFR-PEEK', *Rapid Prototyping Journal*, vol. ahead-of-print, Aug. 2021, doi: 10.1108/RPJ-11-2020-0288.

[73] Alchatek, 'Polyurethane Crack Injection Pumps', Alchatek. Accessed: Dec. 03, 2024. [Online]. Available: https://alchatek.com/equipment/crack-injection-grout-pump/

[74] H. Zhang, W.-Z. Fang, Y.-M. Li, and W.-Q. Tao, 'Experimental study of the thermal conductivity of polyurethane foams', *Applied Thermal Engineering*, vol. 115, pp. 528–538, Mar. 2017, doi: 10.1016/j.applthermaleng.2016.12.057.

[75] G. Tibério Cardoso, S. Claro Neto, and F. Vecchia, 'Rigid foam polyurethane (PU) derived from castor oil (*Ricinus communis*) for thermal insulation in roof systems', *Frontiers of Architectural Research*, vol. 1, no. 4, pp. 348–356, Dec. 2012, doi: 10.1016/j.foar.2012.09.005.

[76] A. Zhang and Y. Li, 'Thermal Conductivity of Aluminum Alloys—A Review', *Materials (Basel)*, vol. 16, no. 8, p. 2972, Apr. 2023, doi: 10.3390/ma16082972.

[77] A. A. Adediran, A. A. Akinwande, O. A. Balogun, O. S. Adesina, A. Olayanju, and T. Mojisola, 'Evaluation of the properties of Al-6061 alloy reinforced with particulate waste glass', *Scientific African*, vol. 12, p. e00812, Jul. 2021, doi: 10.1016/j.sciaf.2021.e00812.

[78] A. M. Dwyer Cianciolo *et al.*, 'Entry, Descent and Landing Systems Analysis Study: Phase 1 Report', NASA, NASA Center for AeroSpace Information,7115 Standard Drive Hanover, 7115 Standard Drive, Hanover, MD 21076-1320, NASA/TM-2010-216720, Jul. 2010.

[79] C. White *et al.*, 'dsmcFoam+: An OpenFOAM based direct simulation Monte Carlo solver', *Computer Physics Communications*, vol. 224, pp. 22–43, Mar. 2018, doi: 10.1016/j.cpc.2017.09.030.

[80] G. Bailet, 'Radiation and ablation studies for in-flight validation', Jan. 2019. Accessed: Dec. 14, 2024. [Online]. Available: https://www.semanticscholar.org/paper/Radiation-and-ablation-studies-for-in-flight-Bailet/078be68aee30aa8fc737526a9cc6f7137c373151

[81] Howard D. Curtis, *Orbital Mechanics for Engineering Students*, Third. Boston: Butterworth-Heinemann, 2014. Accessed: Feb. 02, 2025. [Online]. Available: https://shop.elsevier.com/books/orbital-mechanics-for-engineering-students/curtis/978-0-12-824025-0

[82] Robert A. Braeunig, 'Basics of Space Flight: Orbital Mechanics', Rocket adn Space Technology. Accessed: Feb. 02, 2025. [Online]. Available: http://www.braeunig.us/space/orbmech.htm

[83] K. Bhaskar and T. K. Varadan, *Plates: Theories and Applications*. New York: John Wiley & Sons, Incorporated, 2014. Accessed: Jul. 02, 2021. [Online]. Available: http://ebookcentral.proquest.com/lib/gla/detail.action?docID=1727720

[84] T. H. G. Megson, 'Chapter 7 - Stress and Strain', in *Structural and Stress Analysis (Second Edition)*, T. H. G. Megson, Ed., Oxford: Butterworth-Heinemann, 2005, pp. 150–187. doi: 10.1016/B978-075066221-5/50008-4.

[85] K. Sutton and R. Graves, 'A general stagnation-point convective heating equation for arbitrary gas mixtures', NASA, USA, NASA Technical Report (TR) NASA-TR-R-376, Nov. 1971. Accessed: Jul. 14, 2021. [Online]. Available: https://ntrs.nasa.gov/citations/19720003329

[86] T. Timmons, G. Bailet, J. Beeley, and C. McInnes, 'Mars Atmospheric Characterization with a ChipSat Swarm', *Journal of Spacecraft and Rockets*, pp. 1–8, Mar. 2021, doi: 10.2514/1.A34970.

[87] X. Jiang and S. Li, 'Mars atmospheric entry trajectory optimization via particle swarm optimization and Gauss pseudo-spectral method', *Proceedings of the Institution of Mechanical Engineers, Part G: Journal of Aerospace Engineering*, vol. 230, no. 12, pp. 2320–2329, Oct. 2016, doi: 10.1177/0954410015622230.

[88] H. Amiri *et al.*, 'The Emirates Mars Mission', *Space Science Reviews*, vol. 218, Feb. 2022, doi: 10.1007/s11214-021-00868-x.

[89] 'Hubble Stats', HubbleSite. Accessed: Feb. 03, 2025. [Online]. Available: https://hubblesite.org/home/mission-and-telescope/hubble-stats

[90] G.W. Null, 'F.A Post-Flight Tabulation of the Mariner IV Real-Time Orbit Determination Error', *JPL Spac Program Summary No. 37*, vol. III, no. 39, pp. 24–30, May 1966.

[91] P. J. Mohr, D. B. Newell, and B. N. Taylor, 'CODATA Recommended Values of the Fundamental Physical Constants: 2014*', *Journal of Physical and Chemical Reference Data*, vol. 45, no. 4, p. 043102, Nov. 2016, doi: 10.1063/1.4954402.

[92] D. Lichodziejewski *et al.*, 'Design and Testing of the Inflatable Aeroshell for the IRVE-3 Flight Experiment', in *53rd AIAA/ASME/ASCE/AHS/ASC Structures, Structural Dynamics and Materials Conference*, American Institute of Aeronautics and Astronautics. doi: 10.2514/6.2012-1515.